International Journal of Nanomedicine

Dovepress
open access to scientific and medical research

Open Access Full Text Article

ORIGINAL RESEARCH

A Novel Nanoemulsion Formula for an Improved Delivery of a Thalidomide Analogue to Triple-Negative Breast Cancer; Synthesis, Formulation, Characterization and Molecular Studies

Noran M Tawfik[1,2], Mohammed S Teiama[3,4], Sameh Samir Iskandar[5], Ahmed Osman[1,6], Sherif F Hammad[7,8]

[1]Biotechnology Program, Basic and Applied Sciences Institute, Egypt-Japan University of Science and Technology, Alexandria, Egypt; [2]Department of Zoology, Faculty of Science, Suez Canal University, Ismailia, Egypt; [3]Department of Pharmaceutics and Industrial Pharmacy, Faculty of Pharmacy, Helwan University, Cairo, Egypt; [4]Department of Pharmaceutics, Faculty of Pharmacy, Galala University, Suez, Egypt; [5]Fellow and Head of Surgical Oncology Department, Ismailia Teaching Oncology Hospital (GOTHI), Ismailia, Egypt; [6]Department of Biochemistry, Faculty of Science, Ain Shams University, Cairo, Egypt; [7]PharmD Programs, Egypt-Japan University of Science and Technology, Alexandria, Egypt; [8]Department of Pharmaceutical Chemistry, Faculty of Pharmacy, Helwan University, Cairo, Egypt

Correspondence: Noran M Tawfik; Ahmed Osman, Biotechnology Program, Basic and Applied Sciences Institute, Egypt-Japan University of Science and Technology, New Borg El-Arab, Alexandria, 21934, Egypt, Email noran.tawfik@ejust.edu.eg; ahmed.osman@ejust.edu.eg

Background: Thalidomide (THD) and its analogues were recently reported as a promising treatment for different types of solid tumors due to their antiangiogenic effect.

Methods: In this work, we synthesized a novel THD analogue (TA), and its chemistry was confirmed with different techniques such as IR, mass spectroscopy, elemental analysis as well as ^{1}H and ^{13}C NMR. To increase solubility and anticancer efficacy, a new oil in water (O/W) nanoemulsion (NE) was used in the formulation of the analogue. The novel formula's surface charge, size, stability, FTIR, FE-TEM, in vitro drug release and physical characteristics were investigated. Furthermore, molecular docking studies were conducted to predict the possible binding modes and molecular interactions behind the inhibitory activities of the THD and TA.

Results: TA showed a significant cytotoxic activity with IC_{50} ranging from 0.326 to 43.26 µmol/mL when evaluated against cancerous cells such as MCF-7, HepG2, Caco-2, LNCaP and RKO cell lines. The loaded analogue showed more potential cytotoxicity against MDA-MB-231 and MCF-7-ADR cell lines with IC_{50} values of 0.0293 and 0.0208 nmol/mL, respectively. Moreover, flow cytometry of cell cycle analysis and apoptosis were performed showing a suppression in the expression levels of TGF-β, MCL-1, VEGF, TNF-α, STAT3 and IL-6 in the MDA-MB-231 cell line.

Conclusion: The novel NE formula dramatically reduced the anticancer dosage of TA from micromolar efficiency to nanomolar efficiency. This indicates that the synthesized analogue exhibited high potency in the NE formulation and proved its efficacy against triple-negative breast cancer cell line.

Keywords: thalidomide analogue, antiangiogenic, nanoemulsion, cytotoxicity, triple-negative breast cancer, docking study

Introduction

Advanced breast cancer is hard to treat since it is the most complex heterogenous recurrent disease in females. Suppressing progression and prolongation of survival time is the main goal of clinical intervention.[1] Its rigidity is due to rapid metastasis, which is responsible for over 90% of mortality cases in patients.[2] It is generally divided into different subtypes depending on the molecular expression of hormonal receptors; estrogen receptor (ER), progesterone receptor (PR) and human epidermal growth factor receptor-2 (HER-2). The most aggressive type of breast cancer is the triple-

Received: 5 August 2022
Accepted: 20 December 2022
Published: 11 March 2023

Graphical Abstract

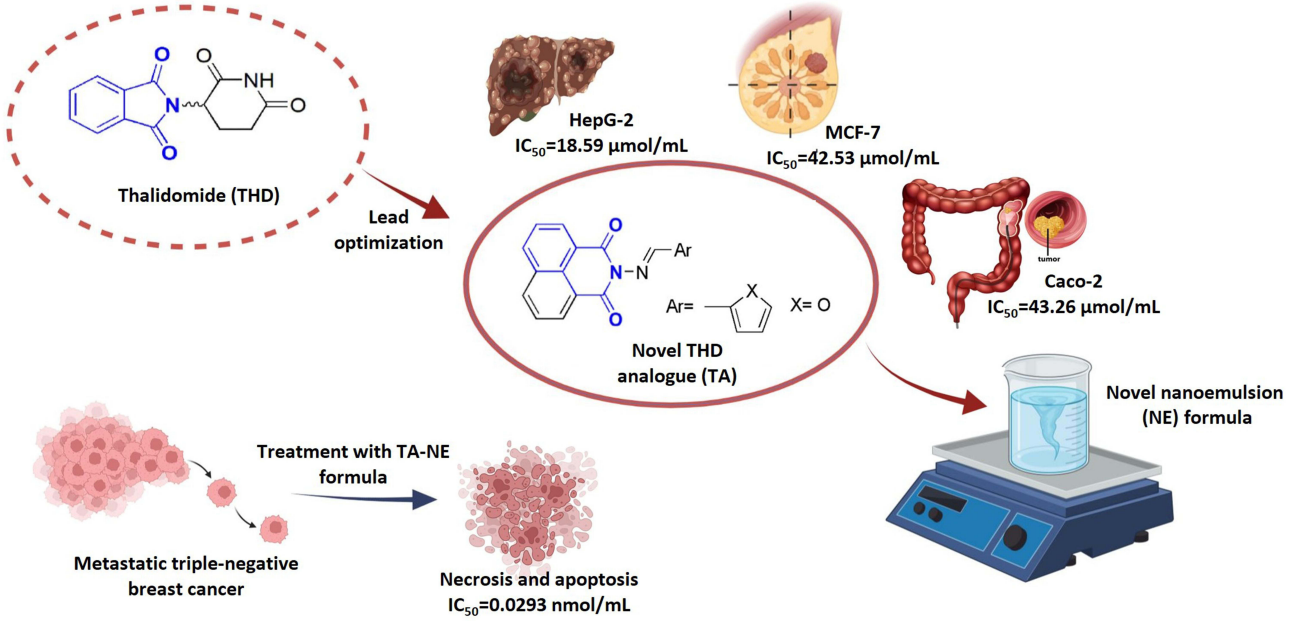

negative, as it lacks the expression of hormonal receptors; therefore, it can be handled and treated only with chemotherapy.[3]

Indeed, the main problems with conventional therapy for triple-negative breast cancer are poor bioavailability and solubility and the development of resistance with adverse side effects on normal cells.[4] Angiogenesis, as one of the significant cancer hallmarks, plays a crucial part in the formation of new vasculatures that supply the solid tumor with oxygen and nutrients for growth and hematogenous metastasis. Consequently, it is considered a pivotal step in cancer progression.[5] Therefore, the best strategy to compete triple-negative cells is to suppress the process of angiogenesis, and this can be achieved through the synthesis of antiangiogenic drugs like thalidomide (THD) and its analogues.

THD is a non-barbiturate sedative drug that was first synthesized by the German pharmaceutical company (Chemie Grünenthal) in late 1950.[6] It was mainly prescribed to pregnant women to relieve morning sickness. However, in 1960 it was completely withdrawn from markets due to severe teratogenic effects.[7] In 2006, it was FDA re-approved and repurposed owing to its anti-inflammation, antiangiogenic, inhibition of cell proliferation and apoptosis promotion.[8] Therefore, it was documented to treat a variety of solid tumors, including bladder cancer,[9] lung cancer,[10] hepatocellular carcinoma,[11,12] Kaposi sarcoma,[13] pancreatic carcinoma[14] and multiple myeloma.[7,15]

It was confirmed that THD blocks angiogenesis through stimulating the immune system, inhibiting cancer cell adherence to stromal cells and suppressing the secretion of vascular endothelial growth factor (VEGF), which is a key regulator in cancer invasion and the most important growth factor in angiogenesis.[16] However, the solubility of THD is a major concern as it is a poorly water-soluble drug, a characteristic that represents one of the most challenges in the pharmaceutical applications.[17] Therefore, a nano-drug delivery system is an approach to deliver drugs to their target biological sites without affecting non-target cells. In addition, it overcomes the poor solubility of drugs and their aggregations.[18] Furthermore, nano-drug delivery systems have different types including polymeric nanoparticles, nanoemulsion (NE), liposomes and nanostructure lipid carriers. They are developed to deliver drugs in a controlled release pattern at the site of action with better targeting and lower toxicity on healthy cells.[19]

NEs are colloidal translucent or transparent dispersions with a small droplet size of less than 200 nm.[20] They can encapsulate hydrophobic drugs to form an aqueous formulations to deliver them to the targeted cells.[21] Moreover, they

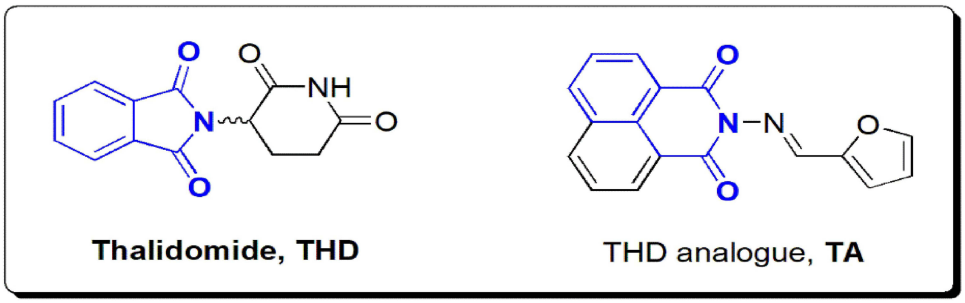

Figure 1 Chemical structures of THD and TA.

protect drugs from enzymatic degradation, improve bioavailability, enhance drug solubility, control drug release and increase drug stability.[20] In addition, they can tolerate the oral route for delivering oral drugs.[22] Furthermore, their small droplet size also inhibits coalescence, and because of their elasticity, surface fluctuations are prohibited.[23]

NE consists of oil, surfactant/co-surfactant (SAA/co-SAA) system and water.[24] SAAs stabilize the small particles by decreasing interfacial tension,[25] increasing surface area and preventing droplets aggregations,[26] while co-SAA forms hydrogen bonds to hold the excess of the aqueous phase.[25] Generally, NEs are classified into different types, and the most common types are oil in water (O/W) NE and water in oil (W/O) NE.[27] Here, we focus on O/W-NE based on non-ionic SAAs that offer stability when tested in vivo for parenteral use.[28] The O/W-NE consists mainly of a core-shell structure, its amphiphilic shell contains SAAs, and its lipophilic core contains the lipophilic non-polar molecule, while the aqueous phase contains the polar solvent.[29]

Indeed, NEs provide specific targeting to cancer cells for efficient tumor treatment. They can also be modified to target the surface of tumor and multidrug-resistant cells. They are effectively taken by tumor cells, minimize toxicity to healthy cells and reduce the spread and migration of tumor cells to other organs.[30] Therefore, NEs could be useful in encapsulating active drugs to treat breast cancer.[31] NEs can be administrated through different routes like pulmonary, intranasal, ocular, oral, topical and intravenous.[32] Natesan et al[33] encapsulated camptothecin (a poor water-soluble drug) in NE and showed high potency in treating breast cancer.[33] Furthermore, Periasamy et al[34] reported that Nigella sativa essential oil NE induced apoptosis in MCF-7 cancer cells.[34] Moreover, clinical trials using NEs for cancer drug delivery paid great attention as oral curcumin-NE was proposed to reduce joint pain in breast cancer survivors. Additionally, curcumin-NE was described for treating obese women at high risk for developing breast cancer.[30]

It has been proposed that the structural modifications of both glutarimide and phthalimide moieties in THD structure could potentiate the antiangiogenic efficacy. Therefore, a novel THD analogue (TA) was synthesized as shown in Figure 1. It has been assessed for its cytotoxicity against different types of cancer cell lines. Furthermore, a parallel strategy of a stable water-based O/W-NE formula was sought to encapsulate the synthesized TA. To the best of our knowledge, it is the first study to prepare O/W-NE consisting of oleic acid as oil, Tween-80 as SAA, n-propyl alcohol as co-SAA and water. The prepared TA-NE formula was studied regarding its droplet size, zeta potential, entrapment efficiency, drug release pattern and thermodynamic stability. Furthermore, an evaluation of its antiproliferative and antiangiogenic activities on triple-negative breast cancer cell line was performed. Also, its effect on the expression levels of mRNAs encoding TGF-β, MCL-1, VEGF, TNF-α, STAT3 and IL-6 was determined.

Materials and Methods

Materials

High-Capacity cDNA Reverse Transcription Kit, Maxima SYBR green qPCR Master Mix (2x), TRIZOL™ Reagent, DMSO 99.9% and Fetal Bovine Serum (FBS) were purchased from Thermo Fisher Scientific (USA). MTT reagent was purchased from Sigma-Aldrich (USA). Tween-80 and oleic acid were purchased from ADWIC, El Nasr Pharmaceutical Chemicals (Egypt). n-propyl alcohol was purchased from Samir Tech-Chem PVT LTD (India). Annexin V-FITC apoptosis detection kit was purchased from Abcam Inc., Cambridge Science Park, Cambridge (UK). RPMI-1640 was

purchased from Biowest (USA). Trypsin EDTA and DMEM were purchased from Lonza™ BioWhittaker (Switzerland). All cell lines were obtained from ATCC.

Methods

Synthesis and Characterization of Naphthalimide Derivative

In a 50 mL round flask, 0.212 gm (1 mmol) of N-aminonaphthalimide was added, followed by 20 mL of absolute ethyl alcohol. Then, 0.12 mL (1.5 mmol) of Furan-2-carboxaldehyde was added, followed by 4 drops of acetic anhydride. The mixture was kept under reflux at 90°C with stirring for 6 h on a hot plate stirrer (Jenway 1000, UK). After that, a sample was taken for a thin layer chromatography (TLC) check that showed reaction completion. The reaction mixture was left to cool down at room temperature until a precipitate was formed. The precipitate was filtered off on a filter paper under vacuum, and crystallization was carried out from ethanol 95% in 80% yield after 3 h. The structure of the synthesized TA was elucidated and characterized by IR, Mass spectroscopy, elemental analysis and ^{1}H and ^{13}C NMR.

2-[(2-Furanylmethylene)amino]-1H-Benz[De]isoquinoline-1,3(2H)dione

M.p. 197–199 °C, IR (KBr) 3437, 1653, 1323, 1230, 1184 $cm^{-1;}$ ^{1}H NMR (DMSO-d_6) 6.78–7.80 (m, 1H, Fur. C_4–H), 7.30–7.31 (m, 1H, Fur. C_3–H), 7.83–7.89 (m, 2H, Naphth. $C_{2,6}$-H), 8.08 (m, 1H, Fur. C_5–H), 8.44–8.51 (m, 4H, Naphth. $C_{1,3,6,8}$-H), 8.58 (s, 1H, CH); ^{13}C NMR (DMSO-d_6) δ 112.78 (Fur. C_3, C_4), 119.71 (C_{4a}), 122.23 (C_4, C_5), 126.69 (C_2, C_7), 127.25 (C_{8a}), 130.99 (CH), 131.29 (C_1, C_3, C_6, C_8), 134.52 (Fur. C_5), 147.59 (Fur. C_2), 159.87 (C=O), 160.25 (C=O); EIMS m/z = 290 (M+).

Construction of NE Pseudo-Ternary Phase Diagram

A pseudo-ternary phase diagram was originated through a water titration method at ambient room temperature with the help of Chemix School 8 software that was reported by Chaudhari and Kuchekar.[35] NE was prepared using oleic acid, water and an emulsifying system consisting of Tween-80 as SAA and n-propyl alcohol as co-SAA. Different ratios of SAA to co-SAA were studied (3:1, 2.5:1.5, 1:1, 4:1, 1:1.5, 0.5:4.5, 1:3, 1.5:2.5, 1:4, 1.5:1, 4.5:0.5, 1.5:3.5).

Preparation of TA-NE Formula

NE was prepared with the spontaneous emulsification method that was reported by Aswathanarayan and Vittal[36] with some modifications. It depends mainly on mixing oil, water and emulsifier at a certain temperature by gentle stirring on a hot plate stirrer leading to the entrance of the emulsifier to the aqueous phase, causing an increase in the interface between oil and water and hence producing oil droplets.[36] Briefly, 1 mg of TA was dissolved in DMSO, then mixed with oil, water and SAA/co-SAA mixture. As reported by Tsai et al,[37] SAA reduces the interfacial tension between the aqueous and the oily phases, and co-SAA offers a further reduction in the interfacial tension. Moreover, co-SAA decreases the concentration of SAA used during the preparation process.[37] In the absence or low concentration of co-SAA, the SAA is likely unable to adequately reduce the O/W interfacial tension.[38]

The prepared NE formula was sonicated and degassed for 30 min with a sink sonicator (Elmasonic S, Germany) to allow the formula to be homogenous, reach equilibrium and disrupt any formed aggregates.[39] Moreover, ultrasonication is an efficient method to reduce NE droplet size.[40] The appropriate oil and SAA/co-SAA ratio used in NE was chosen from the constructed phase diagram. Different formulae (S1, S2 and S3) were chosen from the constructed triphasic diagram. The percentages of the SAA/co-SAA system to the total plain formula were 47%, 32% and 26%, respectively. Then, one formula (S1) was selected for its stability to complete the characterization and the biological study.

Characterization of TA-NE Formula

Droplet Size and Zeta Potential Measurements

The average droplet size, zeta potential and size distribution of the plain NE and TA-NE formulae were determined using dynamic light scattering (Malvern Nano ZS Zeta-sizer, UK). Data analysis was performed using Malvern Zeta-Sizer software version 7.02. All samples were measured at room temperature (25–30°C), where 10 µL of the sample was diluted with 10 mL of distilled water and then sonicated for 15 min with a sink sonicator (Elmasonic S, Germany).

Morphology and Phase Structure Examination

The morphology and phase structure of the plain NE and TA-NE formulae were examined with the field emission transmission electron microscopy FE-TEM (JEOL JEM-2100F, Japan). Samples were placed on a copper grid[41], then 5 μL of phosphotungestic acid was added to provide good staining. Photos were captured with different magnifications.

Drug-Excipients Interaction Study by Fourier Transform Infrared

FTIR spectra of the prepared plain NE and TA-NE formulae were recorded to reveal the functional groups of the drug and excipients of formula to detect any possible interactions between the TA and the components of the NE formula. Formulae were subjected to FTIR (VERTEX 70v FTIR Spectrometer, UK) in the scanning range 4000–500 cm^{-1}.

Thermodynamic Stability Study

Different destabilization mechanisms affect the thermodynamic stability of NE such as flocculation, gravitational separation, creaming and coalescence as reported by Choi and McClements.[42] The plain NE and TA-NE formulae were assessed for their thermodynamic stability through the centrifuge stress and freeze-thaw cycle stress tests. In the centrifuge stress test, the formulae were centrifuged at 13,000 rpm for 30 min with a benchtop microcentrifuge (Sigma, Germany). In the freeze-thaw cycle stress test, the formulae were subjected to three freeze-thawing cycles. Each cycle consists of 24 h at 37°C followed by 24 h at -20°C. Then, the formulae were examined for phase separation, creaming, cracking and precipitation.

Stability Study

Plain NE and TA-NE formulae were tested for long-term stability after storage for 1 year at room temperature (25–30°C) and relative humidity (59–67%). Then, they were checked for phase separation and optical clarity by visual inspection as well as measuring their droplet size and zeta potential. As reported by Wu group,[43] they tested the long-term stability of NE after 1 year of preparation stored at room temperature by measuring their average droplet size and examining their physical characteristics.[43] Alliod et al[44] measured the droplet size and zeta potential for their NE after 9 months of storage at room temperature.[44] Furthermore, Sarheed et al[39] measured NE droplet size after 6 months of storage at room and cool temperature. Moreover, they noticed the physical characteristics of their formulae throughout the storage period at room temperature.[39]

Drug Entrapment Efficiency

The percentage of TA entrapment efficiency was determined in the prepared formula using Equation 1. It was measured using a UV/VIS Spectrophotometer (Perkin Elmer Lambda EZ 201, UK) at 368 nm.

$$\frac{\text{Practical drug loading}}{\text{Theoretical drug loading}} \times 100 \quad (1)$$

In Vitro Drug Release Study

An equivalent of the formula containing 100 μg of TA was loaded into a cellulose dialysis membrane. The dialysis tube was sealed and soaked in 10 mL of distilled water to cover the sink condition. At fixed time intervals (0 min., 30 min., 1 h, 1.5 h, 2 h, 2.5 h, 3 h, 3.5 h, 4 h, 4.5 h, 5 h, 6 h, 7 h, 8 h, 9 h, 10 h, 11 h, 12 h, 24 h and 48 h) following each dialysis time point, about 1 mL of the dialysis media was withdrawn and immediately substituted with an equal volume of distilled water to maintain the volume of the release medium constant throughout the release study. The withdrawn samples were examined for drug concentration by UV/VIS Spectrophotometer (Perkin Elmer Lambda EZ 201, UK) at 368 nm.

Drug Release Kinetics and Mechanism

To study the kinetic profile of TA released from the NE formula, the in vitro release data were fitted to various model kinetic equations such as zero-order (cumulative percentage of drug released versus time), first-order (log cumulative percentage of drug released versus time), Higuchi's model (cumulative percentage of drug released versus square root of time) and Korsmeyer-Peppas model (log cumulative percentage of drug released versus log time). The correlation

coefficient (R^2) for each model was determined, and the best-fitting model was selected that has the highest correlation coefficient (R^2) value.[45] Moreover, the *n* value represents the mechanism of TA released from the formulation. It was determined from the slope of the plotted log time versus log cumulative release percentage (≤60%), where $n \leq 0.45$ indicates a Fickian diffusion mechanism, $0.45 < n < 0.89$ indicates a non-Fickian anomalous diffusion, $n = 0.89$ indicates a case II transport and $n > 0.89$ indicates a super case II transport.

In Vitro Cytotoxicity Studies

Cytotoxic activity of the TA was tested on normal human lung fibroblast cell line (WI-38) as well as it was screened on different types of cancer cell lines; liver hepatocellular carcinoma (HepG2), colorectal adenocarcinoma (Caco-2), breast cancer (MCF-7), androgen-sensitive prostate adenocarcinoma (LNCaP) and poorly differentiated colon carcinoma (RKO). Furthermore, plain NE and TA-NE formulae were tested on the triple-negative breast cancer cell line (MDA-MB-231). Moreover, the TA-NE formula was tested on a multidrug-resistant breast cancer cell line (MCF-7-ADR).

Cell lines were sub-cultured in DMEM or RPMI-1640 medium-containing 10% fetal bovine serum (FBS). 96 well tissue culture plates were inoculated with 1×10^5 cells/mL (100 µL/well) and incubated at 37°C in a 5% CO_2 incubator for 24 h,[46,47] followed by the addition of serial dilutions of TA or the prepared formulae and incubated for an additional 72 h.[46] The effect of treatments on cell viability was examined by MTT assay according to the method of van Meerloo et al.[48] The absorbance was measured using a microplate reader (BMG LabTech, Germany) at 570 nm. The effective concentration of the tested TA and the prepared formulae that caused 50% cell death (IC_{50}) was estimated by the GraphPad Prism 8.0.1 software.

Flow Cytometric Studies

Cell Cycle Analysis

After treatment of the MDA-MB-231 cell line with the determined IC_{50} of the TA-NE formula, treated cells were collected by trypsinization and washed with ice-cold PBS (pH 7.4). Cells were resuspended in 2 mL of 60% ice-cold ethanol and fixed by incubation at 4°C for 1 h. After fixation, cells were washed twice again with PBS (pH 7.4) and resuspended in 1 mL of PBS containing 50 µg/mL RNAase A and 10 µg/mL propidium iodide (PI).[49] After 20 min of incubation in the dark at 37°C, cells were analyzed for DNA contents using flow cytometry analysis using FL2 ($\lambda_{ex/em}$ 535/617 nm) signal detector (ACEA Novocyte™ flow cytometer, ACEA Biosciences Inc., USA). For each sample, 12,000 events were acquired. ACEA NovoExpress™ software (ACEA Biosciences Inc., USA) was used to evaluate cell cycle distribution. The experiment was performed three independent times.

Annexin V Apoptosis Assay

Necrotic and apoptotic cell populations were determined using Annexin V-FITC apoptosis detection kit (Abcam Inc., Cambridge Science Park, Cambridge, UK) coupled with 2 fluorescent channels flow cytometry. After treatment of the MDA-MB-231 cell line with the determined IC_{50} of TA-NE formula, treated cells (10^5 cells) were collected by trypsinization and washed twice with ice-cold PBS (pH 7.4). Subsequently, cells were incubated with 0.5 mL of Annexin V-FITC/PI solution for 30 min in the dark at room temperature according to manufacturer's protocol. After that, cells were subjected to ACEA Novocyte™ flow cytometer (ACEA Biosciences Inc., USA) and screened for FITC and PI fluorescent signals using FL1 and FL2 signal detectors, respectively ($\lambda_{ex/em}$ 488/530 nm for FITC and $\lambda_{ex/em}$ 535/617 nm for PI). For each sample, 12,000 events were detected, and positive FITC and/or PI cells were examined by quadrant analysis and calculated using ACEA NovoExpress™ software (ACEA Biosciences Inc., USA).

Quantitative RT-PCR

Total RNA was extracted from untreated and TA-NE treated MDA-MB-231 cell line by TRIZOL™ Reagent according to the manufacturer's protocol. RNA concentration and purity were determined by nanodrop (A_{260} and A_{280}) (Thermo Fisher Scientific 2000c, USA). All the mRNA were reverse transcribed to cDNA by High-Capacity cDNA Reverse Transcription Kit (Thermo Fisher Scientific, USA) according to the manufacturer's instructions. qPCR reaction was conducted for TGF-β, MCL-1, VEGF, TNF-α, STAT3 and IL-6 genes using Thermo Scientific Maxima SYBR Green qPCR Master Mix (Thermo Fisher Scientific, USA). The primers used are listed in Table 1. Thermal cycling conditions for amplification of all primers were a three-step cycling protocol except for IL-6 was a two-step cycling protocol. The

Table 1 Primers Sequences for qRT-PCR

Gene	Forward Primer	Reverse Primer
TGF-β	5' AATTCCTGGCGATACCTCAGCA 3'	5' TGAACCCGTTGATGTCCACTTG 3'
MCL-1	5' CGGCAGTCGCTGGAGATTATCT 3'	5' TTGATGTCCAGTTTCCGAAGCAT 3'
VEGF	5' AAGGAGGAGGGCAGAATCATC 3'	5' CAGGATGGCTTGAAGATGTACT 3'
TNF-α	5' TCCAGGCGGTGCTTGTTCCT 3'	5' AGAGGGCTGATTAGAGAGAGG 3'
STAT3	5' AGGAGGAGGCATTCGGAAAGT 3'	5' TGTCACACAGATAAACTTGGTCT 3'
IL-6	5' AGTACCTCCAGAACAGATTTG 3'	5' GCATTTGTGGTTGGGTCAGG 3'
HPRT-1	5' CTGGCGTCGTGATTAGTGATGAT 3'	5' AGCACACAGAGGGCTACAATGT 3'

qPCR reaction was conducted on QuantStudio™ 5 Real-Time PCR System (Thermo Fisher Scientific, USA). The software utilized was QuantStudio™ Design & Analysis Software v1.5.1. The relative gene expression levels were calculated using the livak method. The data were normalized using HPRT-1 as a housekeeping gene.[50]

In Silico Molecular Docking Studies

Tested Compound Optimization

Docking studies were performed using the Molecular Operating Environment software package (MOE, 2014.10, Chemical Computing Group Inc. Montreal, Canada).[51] We evaluated the activity of THD and TA compared to docked crystallized ligands (WFE, RO4, 3SR and BAX) complexed with the (AKT Kinase, MMP1, ALDH1 and VEGF) proteins, respectively, that act as a binding site inhibitor. THD and TA were drawn on MOE sketcher. Structures of the co-crystallized ligands (WFE, RO4, 3SR and BAX) were downloaded from the drug bank website (https://www.drugbank.ca/). After checking THD, TA and co-crystallized ligands chemical structures and the formal charges on atoms by the 2D depiction, the tested compounds were subjected to energy minimization using Force Field MMFF94x. The partial charges were calculated automatically. Each co-crystallized ligand (WFE, RO4, 3SR and BAX) was imported with THD and TA in a separate database and saved as an MDB file to be utilized in the docking calculations as four separate processes for each protein pocket, respectively.

Protein Active Site Optimization

X-ray crystal coordinates of AKT Kinase (PDB code: 3mvh, in complex with WFE), MMP1 (PDB code: 2TCL, in complex with RO4), ALDH1 (PDB code: 4WP7, in complex with 3SR), VEGF (PDB code: 4ASD, in complex with BAX) were obtained from the Protein Data Bank (http://www.rcsb.org/). The target protein was fully prepared for docking calculations. Hydrogen atoms with their standard 3D geometry were added to the system. To check for any error in the atomic connections and types, an automatic correction was applied. Additionally, the receptors and its atoms' potentials were fixed. Site finder was utilized to select the same active site of the co-crystallized inhibitor in the enzyme structure through utilizing all default items, where dummy atoms were created from the site finder of the pocket.

Docking of Molecules into the Binding Site of Protein

Docking of each database composed of THD, TA and the co-crystallized ligand was performed. The following method was applied: the file of the prepared protein active site was loaded, and the docking tool was commenced as template and general docking processes. The set-up of the program specifications was as follows: triangle matcher is the placement technique, dummy atoms are the docking site, rigid receptor is the refinement methodology, London dG represents the scoring methodology and GBVI/WSA dG is the scoring methodology for the best poses selection. The scoring methods were adjusted to default values. The MDB file of the three ligands in each of the four databases was loaded and automatic general docking calculations were performed. The ligand-enzyme complex scores in kcal/mol were encompassed in the output database. Consequently, the generated docking poses and interactions with binding pocket residues were examined. The superimposition of the binding orientations of docked molecules into the binding pocket with the top scores and exhibiting good ligand enzyme contacts were depicted.

Statistical Analysis

Data were statistically analyzed by Microsoft Excel® 2016, Statistical Package for Social Science (SPSS)® Version 24 and Minitab® statistical software Version 16. Data were revealed as means, standard deviations and standard errors of the mean for further analysis using one-way analysis of variance (ANOVA) followed by Tukey's post hoc test for multiple comparisons. The level of significance was calculated at $P \leq 0.05$.

Results and Discussion

TA Synthesis Process

We aimed to expand on the results of our previous study,[52] Scheme 1 represents the synthesis steps of a novel TA, where N-aminonaphthalimide reacts with Furan-2-carboxaldehyde in the presence of absolute ethyl alcohol and acetic anhydride. The mixture was kept under reflux at 90°C with stirring for 6 h. The reaction mixture was left to cool down at room temperature until a precipitate was formed.

Construction of Pseudo-Ternary Phase Diagram

The pseudo-ternary phase diagram was plotted, as shown in Figure 2. Tween-80, whose use is approved by FDA, was selected as a non-ionic hydrophilic SAA owing to its use in food and medicine as an emulsifying agent. It was reported to increase drug permeability when tested in vitro on Caco-2 colorectal cell line, in vivo (rats) and ex vivo (rat intestinal membrane).[53] Also, oleic acid could be used safely, and it was proven to exhibit some antitumor activity against different types of cancer such as colorectal, breast and prostate cancer.[54]

Figure 2 shows that SAA/co-SAA system succeeded in decreasing the interfacial tension between oleic acid and water, thus facilitating the fabrication of NE droplets (gray area), whereas the white area indicates that the formed system comprises two phases. The borderline between these two areas (gray/white) represents the first visual turbidity during the titration step after the formation of NE. The NE formula was prepared with a low percentage of hydrophilic non-ionic SAA (17%), following the recommendations of Manickam et al,[55] who showed that utilizing low SAA concentration in the NE formulation guarantees that the synthesized formula can be used in pharmaceutical applications.[55]

For producing NE, the SAA concentration should be high enough to stabilize droplets such that low interfacial tension is achieved.[56] An optimal SAA concentration is required to formulate NE, thus preventing oil droplets from aggregation.[57] In our prepared formula, we utilized an adequate concentration of SAA and that was proved by the formation of a small-size stable formula that was transparent and clear. Moreover, the small size of NE was due to the sufficient amount of SAA covering each oil droplet.[58] Azeem group[38] prepared NE consisting of 40 wt.% of SAA to co-SAA.[38] Furthermore, Sarheed et al[39] utilized different SAA to oil ratios (5:1, 7:1, 10:1, 5:2, 7:2 and 10:2). They reported that the high SAA concentration could prevent any form of instability or coalescence. Moreover, they observed no phase separation in their formulae indicating their stability.[39] Furthermore, Shah et al[59] stated that utilizing high concentrations of hydrophilic SAAs in the nanoformulation led to the loss of the dissolution capacity for hydrophobic drugs in the formula upon dilution with water in the gastrointestinal tract, which leads to precipitation of the dissolved drug.[59]

In our study, three formulae (S1, S2 and S3) were chosen from the constructed pseudo-ternary phase diagram, as shown in Figure 3. Then, one formula (S1) was selected for its stability to complete the characterization and the

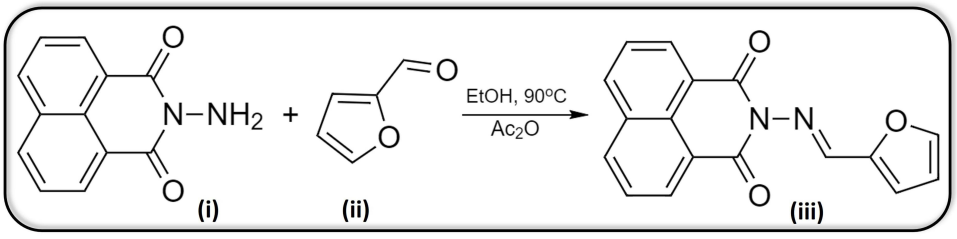

Scheme 1 Synthesis of TA compound, where (i) represents N-aminonaphthalimide, (ii) represents Furan-2-carboxaldehyde, (iii) represents TA, EtOH is absolute ethyl alcohol and Ac_2O is acetic anhydride.

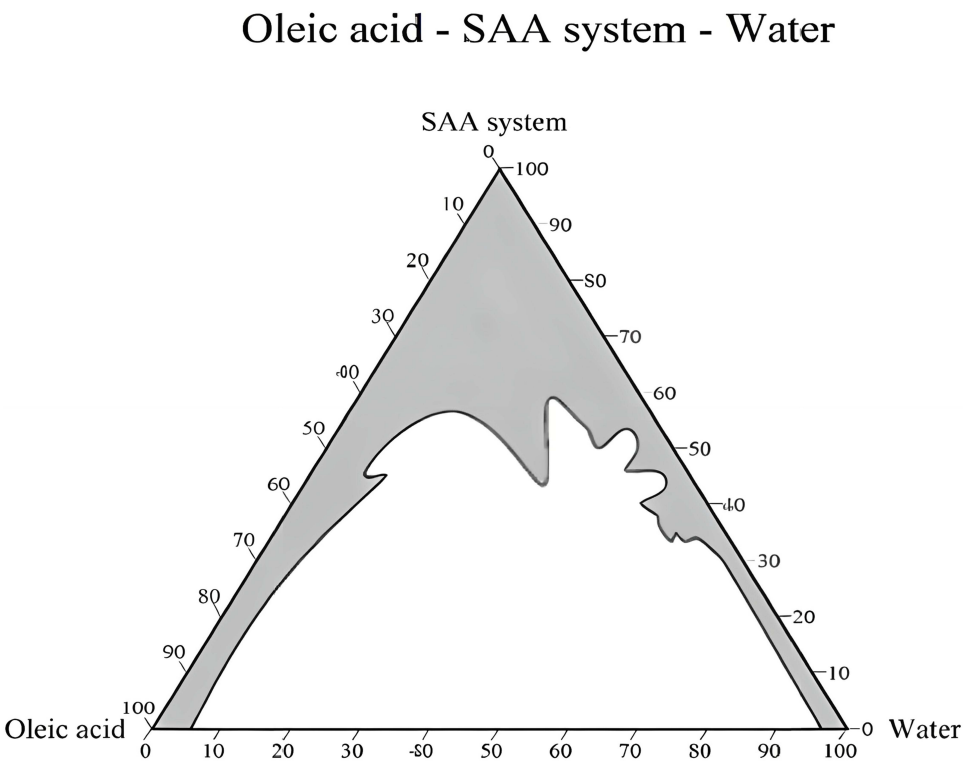

Figure 2 Pseudo-ternary phase diagram of the prepared plain NE consisting of oleic acid, Tween-80, n-propyl alcohol and water. The clear area under the curve shows the multiphase system, while the gray area under the curve shows the one phase system.

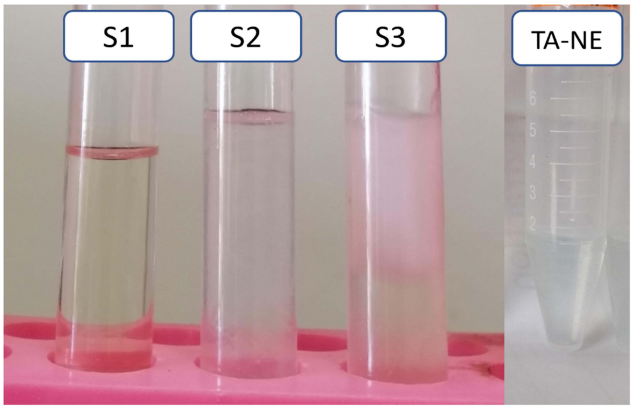

Figure 3 S1, S2 and S3 represent three prepared plain NE formulae. S1 represents the most stable formula as it showed clear transparent formula without any aggregations; S2 and S3 represent unstable formulae as they showed aggregations, phase separations and coagulations; TA-NE formula represents the prepared formula after a year of preparation showing a clear transparent formula.

biological study. The selected formula was optically transparent and showed no visible precipitations during the preparation steps or after storage for 1 year. Handa et al[25] discussed that the transparent NE was due to the fatty acid moiety in the oleic acid attached to the sorbitan moiety in Tween-80, resulting in more steric hindrance.[25] In terms of SAA ratios, our preparation was different from that of Handa et al,[25] who stated that a higher amount of SAA was needed for obtaining a transparent NE formula. In their study, they used pine oil, Tween-80 and PEG400 and increased the ratio of Tween-80:PEG400 from 1:1 to 1:2 and 2:1. They explained their results that the hydroxyl moiety of water was weak and PEG400 was not affordable to hold neither the water molecules nor the hydrogen bond of the glycol moiety.[25]

On the other hand, our NE preparation likely exhibited low interfacial energy due to the adequate ratios of Tween-80/n-propyl alcohol to oil and water. Furthermore, n-propyl alcohol was used as co-SAA in the formulation of NE as alcohols participate in the reduction of water uptake and droplet size due to their weak amphiphilic behavior, as described by Mathew and Juang[60] whereas alcohol molecules such as ethanol and isopropyl participate in the interfacial region of droplets and form a dense SAA system, improving the NE formula's stability.[60] This observation is consistent with the reported results of a study done by Azeem group,[38] who evaluated the effect of different alcohols, such as n-butanol, ethyl alcohol, isopropanol and other polymers (propylene glycol, PEG400 and carbitol) as co-SAAs. They found that co-SAA of short to medium chain lengths (C3–C8) acts to lower interfacial tension, promote interface fluidity and improve the mobility of the hydrocarbon tail, allowing more oil to penetrate this region.[38]

Characterization of TA-NE Formula

Droplet Size Measurements

The mean droplet size measured in distilled water at the time of preparation for plain NE and TA-NE formulae was 345.73±6.84 nm and 372.7±69.37 nm, respectively. Sarheed et al[39] noticed a decrease in droplet size in the oleic acid formulation with an increasing concentration of SAA. They explained this behavior as the SAA could be adsorbed onto the interface between water and oil to minimize interfacial tension and decrease the free energy needed to disrupt the droplets leading to droplet disruption and a decrease in size as the SAAs might form a protective coating around particles resulting in inhibition of coalescence with one another.[39] Wang and Zhang[61] produced NE of approximately 109–139 nm with spherical structure prepared by spontaneous emulsification method.[61]

Polydispersity index (PDI) refers to the distribution of particles in the NE formula. Its value was recorded in correspondence with the values of droplet size. PDI measured in distilled water at the time of preparation of plain NE and TA-NE formulae were 0.618 and 0.517, respectively. This indicates narrow size distribution and excellent homogeneity. As reported by Danaei et al,[62] PDI is a dimensionless value of simple calculation from two different parameters that fits to the cumulants analysis of the correlation data. PDI ranges between 0.05 and 0.7 indicate high monodispersed or a very broad particle size distribution, respectively.[62]

Morphology and Phase Structure Examination

The plain NE and TA-NE formulae were examined with FE-TEM, which showed their fine spherical structure (Figure 4). Pouton[63] stated that very fine dispersions (less than 100 nm) were produced during the preparation of a self-emulsifying system with the use of hydrophilic SAA (40% or more) or co-SAA in addition to SAAs.[63] In our prepared formula, 47% of the SAA/co-SAA was used, which explained the small droplet size.

The clear transparent appearance did not change upon loading of TA. Moreover, the plain NE and TA-NE formulae exhibited a clear transparent appearance. McClements and Rao[29] reported that as the NE size was less than 70 nm, it is controlled by the Brownian motion that affects its movements and thus prevents creaming.[29] These findings agreed with the study of Sarheed et al,[39] who reported that 50% of their O/W-NE droplet size increased upon loading of lidocaine in comparison with the blank NE formula, and there was no change in the physical appearance of their formulations.[39]

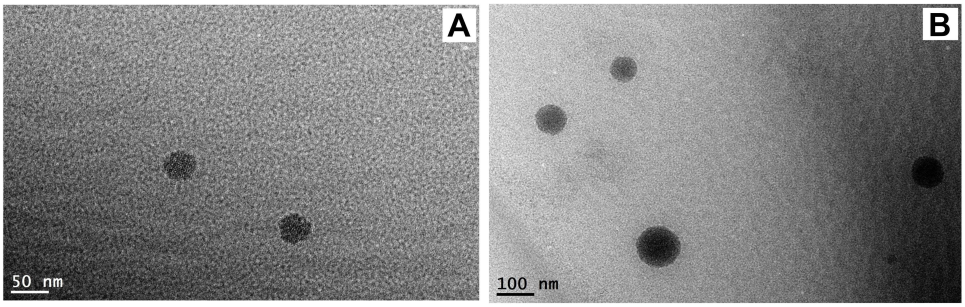

Figure 4 Field Emission Transmission Electron microscope photomicrographs. (**A**) Plain NE formula; (**B**) TA-NE formula.

The particle size measured by the zetasizer has larger values than that measured by FE-TEM. This result was expected as the zetasizer measures the hydrodynamic size of particles, while FE-TEM measures the actual droplet size of particles. These findings were consistent with previous studies.[64,65] Cancer cells are surrounded by vascularized tissues that facilitate the accumulation of NEs in these tissues depending on their small size to pass through barriers.[30] For medical applications, the size of NE particles is important for drug pharmacokinetics, where the recommended mean particle size of NEs is 100–300 nm.[66] It should be noted that the NE particle size should not be too large to avoid blocking of the blood vessels and not too small to be indiscriminately and rapidly absorbed.[67] Sánchez-López et al[30] mentioned that size of NEs in the range of 20–100 nm can pass through blood vessels, accumulate in tumor tissues and are away from renal clearance.[30]

Indeed, Wani et al[68] reported that the small particle size of the NE influences the absorption of the drug and their biological fate.[68] The small size of NEs leads to a higher bioavailability as they can penetrate through the pores in the mucus layer resulting in faster absorption by cells.[68] NEs can be administrated by the intravenous route through the enhanced permeability and retention effect.[69] According to Attia et al,[70] the blood vessels of tumor tissue become more permeable than in healthy tissue. The rapidly expanding tumor engulfs the formed blood vessels or recruits new blood vessels in response to hypoxia.[70] These new vessels are leaky in nature, providing enhanced selective penetration of nanostructures and molecules larger than 40 KDa to the tumor stroma. Moreover, the lack of healthy lymphatic drainage in cancer tissue plays an important role in nanoparticle retention. Furthermore, targeting tumor tissue occurs passively depending on the tumor biology, like leakiness and vascularity.[70,71]

Drug-Excipients Interaction Study

FTIR spectra of the plain NE and TA-NE formulae are shown in Figure 5. It showed no significant change between plain NE and TA-NE formulae. However, it showed the successful loading of TA in the NE formula, where the characteristic peaks of THD were detected in the TA-NE formula. The strong broad peak at 3200–3550 cm^{-1} indicates the presence of (O-H) stretching of NE. The band below 3000 cm^{-1} shows the absorption band for (C-H) stretching. The absorption at 1600 cm^{-1} represents (C-O) stretch. The weak and broad peak at 1520 cm^{-1} characterizes the (C-O-H) of the alcohol. In addition to (N-H) stretch was characterized at 1600 cm^{-1}. For the TA-NE formula, FTIR exhibited a characteristic peak of THD as Jin et al,[72] reported that the (C-H) stretching of the aromatic ring was at the frequency 690–900 cm^{-1}.[72] The (C-H) stretching of the TA was determined at 990–1045 cm^{-1}.

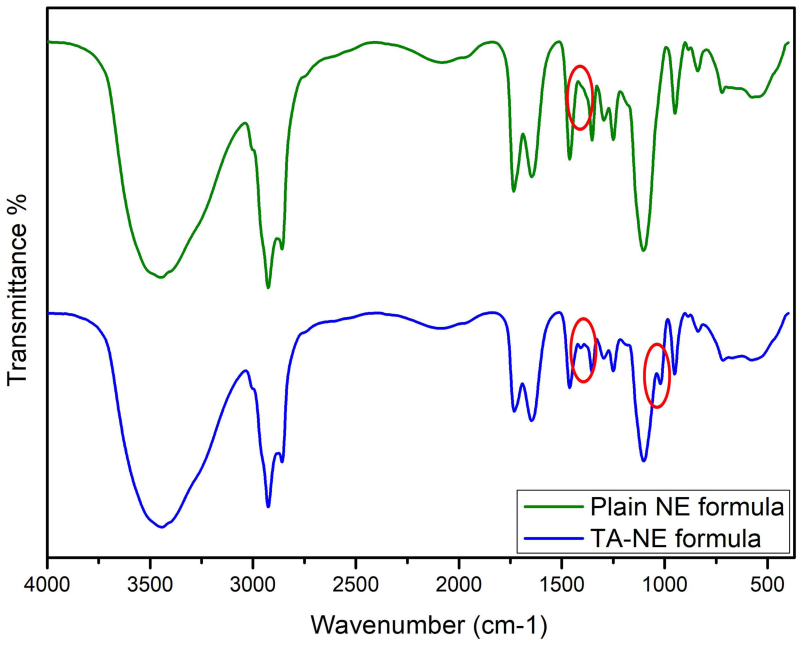

Figure 5 FTIR spectra of the plain NE and TA-NE formulae. The characteristics peak (C–H) stretching of the TA at 990–1045 cm^{-1}, and the weak and broad peak at 1520 cm^{-1} characterizes the (C-O-H) of the alcohol are indicated by red eclipses.

Thermodynamic Stability

Different plain NE formulae were prepared and examined visually to select the most stable one. The selected plain NE formula and TA-NE formula showed no signs of aggregations, creaming or phase separation at the time of preparation and after storage for a year at room temperature (25–30°C) exposed to light and dark conditions. Moreover, they were also stable when exposed to centrifuge stress and freeze-thaw stress tests without any precipitation or change in their physical appearance. Handa et al[25] stated that Tween-80 formulated NE system resulted in an optically clear, transparent and highly stable NE.[25] The prepared formulae have no change regarding their clearance and aggregations, ensuring no Ostwald ripening occurred. As mentioned by Che Marzuki et al,[73] that Ostwald ripening is a destabilization process occurs when two droplets fuse together to form one large droplet. In addition, with enough time, the NE size increases and becomes turbid.[73]

Alliod et al[44] reported that the long-term stability of NE was due to the use of sufficient SAA amount during preparation.[44] The SAA percentage utilized was 17%, which was sufficient for the NE to be formed with a clear and transparent appearance, and it also provided long-term stability for up to a year. Danhier et al[74] mentioned that the final feature of the formulation was affected by the particle size, where the formulation's stability increases as the particle size decreases. This is important against Brownian motion, gravitational force and flocculation.[74]

Stability Study

Regarding the pharmaceutical application of drugs, it was necessary for the prepared formula to have good stability correlated with its corresponding zeta potential values.[75] A stability study was carried out to detect changes in the formulae's droplet size and zeta potential after a year of preparation, where the formulae were stored at room temperature (25–30°C) exposed to light and dark conditions. The mean droplet size after a year of preparation measured in distilled water for the plain NE and TA-NE formulae was 195.4±1.97 nm and 194.93±7.94 nm, respectively, which showed a decrease in the mean droplet size. This can be explained by Aswathanarayan and Vittal,[36] who reported that NEs are exposed to chemical degradation due to their large surface area, which makes them susceptible to hydrolysis and oxidation. Furthermore, the chemical stability of NEs is influenced by their opacity, where the transparent NEs with small droplet size are easily degraded by visible or UV light due to their transparency.[36] Alliod et al[44] reported no significant increase in the average droplet size of NE for 9 months stored at room temperature because the SAA concentration was sufficient for their long-term stability.[44] Moreover, Sarheed et al[39] reported a decrease in their NE droplet size after 6 months of storage at room and cool temperature.[39]

The electrical surface charge or particle charge was determined by measuring the zeta potential at the time of preparation and after storage for a year. Zeta potential values at the time of preparation of the plain NE and TA-NE formulae were -47.2±0.4 mV and -40.13±1.27 mV, respectively. Interestingly, after storage for a year, the values of zeta potential of the plain NE and TA-NE formulae were -46.63±2.28 mV and -32.13±0.63 mV, respectively. It showed insignificant change before and after storage for the plain NE formula, while showing significant change ($p<0.01$) for TA-NE formula; however, the charge is still within the accepted values (>-30 mV or >+30 mV) that indicates a high stability pattern of the formulae after storage for a year.

To sum up, the values of zeta potential for the plain NE and TA-NE formulae were with a high negative surface charge at the time of preparation and after storage for a year. Rodrigues et al[76] discussed that the high negative charge for the NE formula showed a high stability pattern upon storage since repulsions between droplets surpassed the attraction forces that prevent coalescence and coagulation of the colloidal particles.[76] These results agreed with the results reported by Sobhani et al,[26] where they stated that as the value of the zeta potential increased towards negative or positive (-30 mV to +30 mV), the net charge of the droplets increased, which offers more stabilization in the NE.[26] It was reported that when the zeta potential value was more negative than 30 mV, this indicates a high electrical stability due to electrostatic repulsion that prevents droplets aggregations resulting in physical stability of NE.[39] Tran et al[77] mentioned that a nano drug-delivery system exhibiting a medium negative charge value (approx. -20 mV) or completely negative charge value (≤-30 mV) showed improved physiological and physical stability in blood and could enhance the drug half-life inside the blood circulation.[77] Furthermore, Wang and Zhang[61] prepared NE with zeta potential ranging between -38.5 mV and -28.5 mV.[61]

Drug Entrapment Efficiency and In Vitro Drug Release Study

The drug entrapment efficiency for TA inside the formula was 99.33%. This high value was due to the low surface tension among NE droplets that inhibits their coalescence and this was assured by the absence of phase separation, which enhanced drug retention and solubility in the formula.[39] The dialysis membrane used was of molecular weight cut-off 12–14 kDa, and the molecular weight of TA was 290.07 g/mol. Kang et al[78] reported that this cut-off was to retain the formula inside the membrane, allow only the drug to transfer to the release media and reduce the effect of membrane during the release process.[78] According to Xu et al,[79] the dialysis membrane cut-off value should be 100 times the drug's molecular weight.[79]

The release pattern for the TA from NE formula (Figure 6) showed that 29.1±1.21% was released after 2 h, 42.26 ±0.25% was released after 4 h, 65±0.27% was released after 12 h, 87.3±11.84% was released after 24 h, and finally, the release was completed after 48 h. Therefore, the prepared formula exhibited an extended-release pattern, which maintains the drug level for a longer time inside the blood circulation and improves patient control. Araújo et al[80] dissolved THD in acetonitrile solution; therefore, they used ammonium acetate as a release medium from the parenteral NE formula. They found that more than 80% of THD was released to the release media after 2 h.[80] Partitioning of the drug from the oil phase into the SAA layer and then into the aqueous phase is the sequence by which the drug is released from NE. During diffusion from oil, the solubilized drug moiety comes first into contact with the aqueous phase and undergoes nanoprecipitation. This greatly increases the drug's surface area, hastening its disintegration.[81]

Drug Release Kinetics and Mechanism

The highest value of R^2 represents the release kinetics for the formula. The R^2 values for zero order, first order, Higuchi's model and Korsmeyer-Peppas model were 0.7313, 0.5108, 0.9221 and 0.9693, respectively. The in vitro release data were best fitted to the Korsmeyer-Peppas model. It reveals that the release of the drug from the formula may be due to the swelling of the formula or diffusion of water inside. Moreover, the exponent *n* value was 0.48, indicating a non-Fickian diffusion release mechanism.

In Vitro Cytotoxicity Studies

TA revealed its safety on the proliferation of normal human cell line (WI-38) with an IC_{50} of 101.01 µmol/mL. WI-38 cell line was selected according to literatures, as mentioned by Chen et al,[82] that the most common sites of breast cancer metastases are bones (65.1%) followed by lungs (31.4%).[82] Metastatic spread of breast cancer commonly attacks bones and lungs.[83,84] Table 2 indicates that TA exhibited antitumor activity in micromolar concentration on different cancer cell lines. Interestingly, the encapsulation of the TA in the NE formula enhanced its antitumor potency and decreased the IC_{50} to nanomolar concentration.

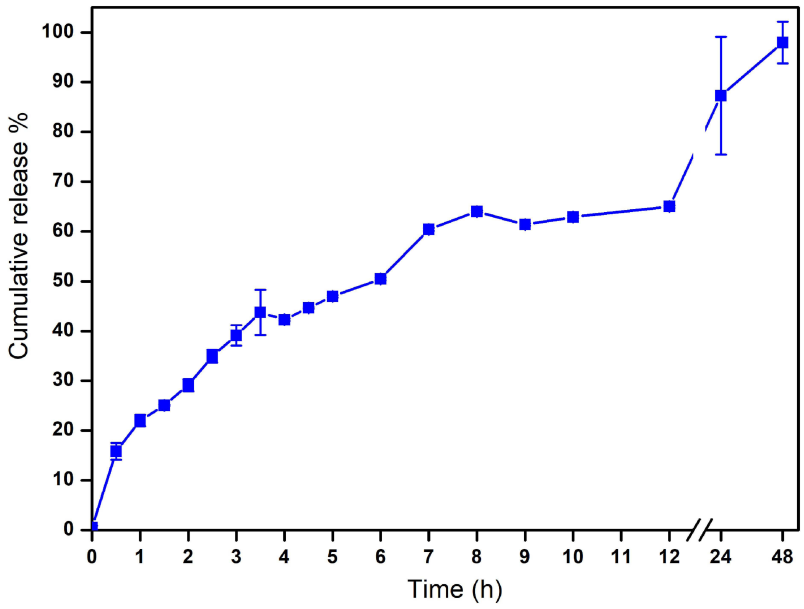

Figure 6 In vitro drug release study for TA from NE. It revealed that complete release was achieved within 48 h.

Table 2 Cytotoxicity Studies of TA and TA-NE Formula on Different Types of Cell Lines

Tested Sample	Cell Lines	IC_{50}
TA	Normal human lung fibroblast cell line (WI-38)	101.01 µmol/mL
	Liver hepatocellular carcinoma cell line (HepG2)	18.59 µmol/mL
	Colorectal adenocarcinoma cell line (Caco-2)	43.26 µmol/mL
	Breast cancer cell line (MCF-7)	42.53 µmol/mL
	Androgen-sensitive prostate adenocarcinoma cell line (LNCaP)	0.326 µmol/mL
	Poorly differentiated colon carcinoma cell line (RKO)	1.096 µmol/mL
TA-NE formula	Triple-negative breast cancer cell line (MDA-MB-231)	0.0293 nmol/mL
	Multidrug-resistant breast cancer cell line (MCF-7-ADR)	0.0208 nmol/mL

TA-NE formula showed an IC_{50} of 0.0293 nmol/mL (equivalent to 8.509 ng/mL) on MDA-MB-231 cells and 0.0208 nmol/mL (equivalent to 6.058 ng/mL) on MCF-7-ADR cells, demonstrating high anticancer activity. The plain NE formula showed an IC_{50} of 49.42 ng/mL on MDA-MB-231 cells. Figure 7 indicates that the anticancer activity on MDA-MB-231 cells is dose-dependent. The most relevant finding is that the nanoformulation of the TA dramatically reduced the anticancer dosage from micromolar efficiency to nanomolar efficiency. The TA-NE formula has more cytotoxic activity and is a more promising anticancer agent on the metastatic triple-negative cell line.

Flow Cytometric Studies

Cell Cycle Analysis

Cell cycle analysis was assayed to assess the effects of TA-NE treatment of MDA-MB-231 cells with the determined IC_{50} of TA-NE formula at different phases of cell cycle such as sub G1, G0/G1 phase, S-phase and G2/M phase as compared to that of untreated cells. Figure 8 indicates that treatment of MDA-MB-231 cells resulted in a significant increase ($p<0.05$) in cell population in the G2/M phase, which indicates that TA-NE formula induced cell cycle arrest in the G2/M phase compared to that of untreated cells. Our findings agreed with Marriott et al[85] who showed that their second generation of the synthesized TAs promoted cell cycle arrest at G2/M phase at a concentration of 50 µg/mL for 48 h in different types of cancerous cells such as colorectal (SW620), pancreatic (BxPC-3), prostate (PC-3) and melanoma (MJT-3) cell lines.[85] Furthermore, El-Zahabi et al[86] demonstrated that THD induced apoptosis in the colorectal carcinoma (HCT-116) cell line in the G2/M phase at a concentration of 10 µM for 24 h.[86] On the contrary, these findings were in contrast with the data reported by Zhu et al,[87] as they concluded that THD enhanced the cell cycle arrest

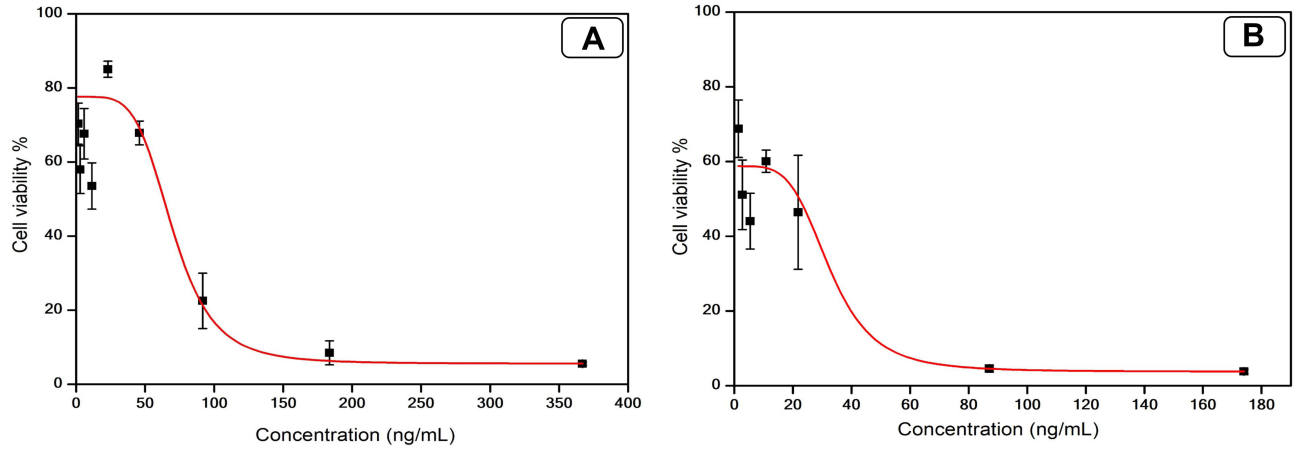

Figure 7 Cytotoxicity study on MDA-MB-231 cell line representing the IC_{50} values. (**A**) Plain NE formula (49.42 ng/mL); (**B**) TA-NE formula (8.509 ng/mL).

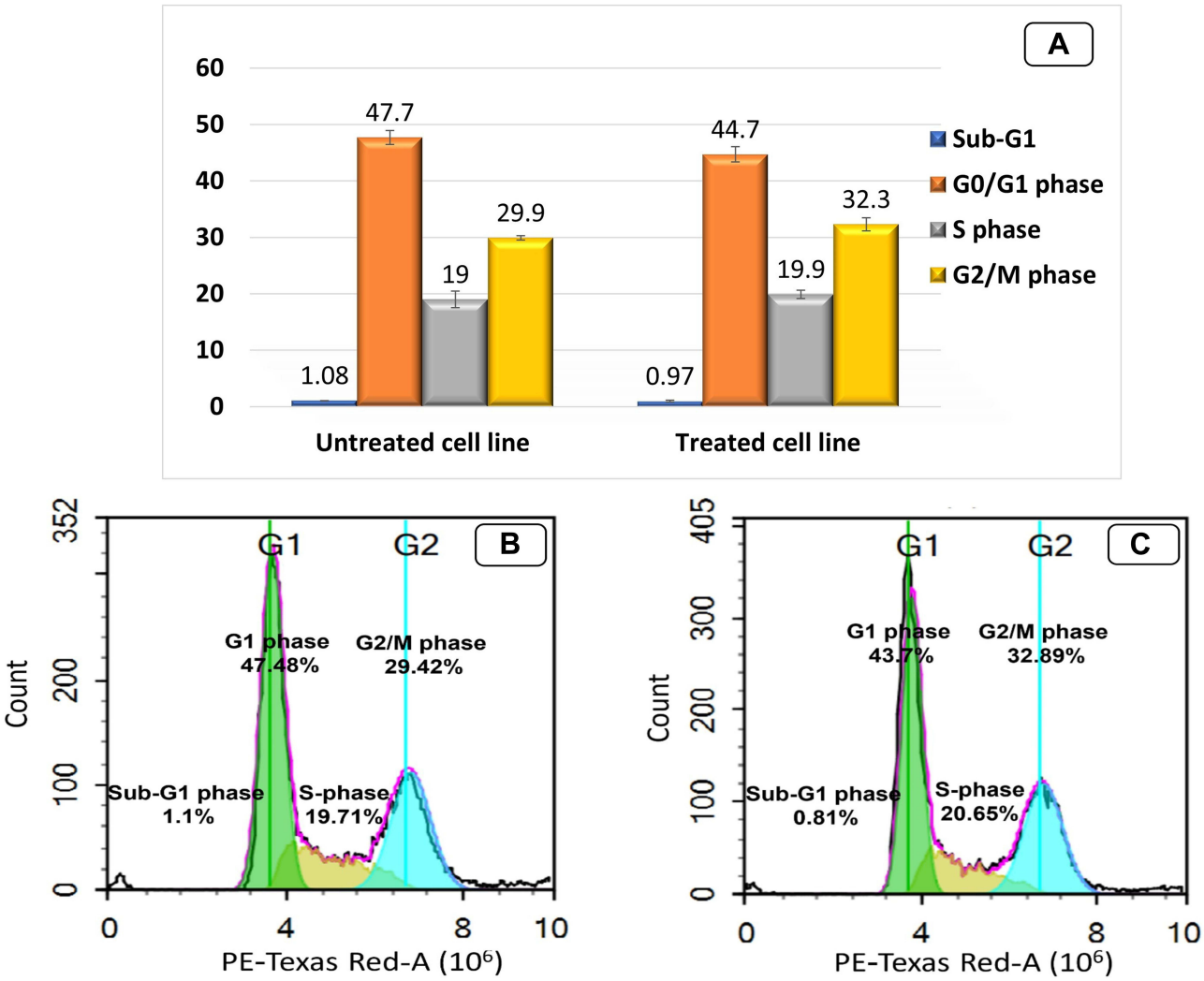

Figure 8 Cell cycle analysis of untreated MDA-MB-231 cell line (control) and treated MDA-MB-231 cell line with TA-NE formula. (**A**) The bar graph represents the percentage values of cells in each stage of cell cycle. TA-NE formula induced cell cycle arrest in the treated MDA-MB-231 cell line significantly in G2/M phase compared to that of untreated cells; (**B**) Untreated MDA-MB-231 cell line; (**C**) Treated MDA-MB-231 cell line with TA-NE formula.

of the human osteosarcoma (MG-63) cell line by increasing the cell population in the G0/G1 phase and decreasing the cell percentage in S phase at an incubation of 0, 50, 100 and 200 µg/mL when cells were treated for 48 h.[87] Also, Tokunaga et al[88] disagreed with our results and showed that their synthesized analogue (fluoro-THD) induced cell cycle arrest at G1 phase, while it decreased cell population in the S-phase in the multiple myeloma (H929) cell line when treated at a concentration of 20 µg/mL for 24 h.[88] Moreover, Kian group[89] came in contrast with ours and concluded that THD induced cell cycle arrest in the bone marrow (KG-1) and myeloid leukemia (U937) cell lines in G0 and S phases of the cell cycle at IC_{50} of 80 µM and 60 µM in KG-1 and U937 cells, respectively, when cells were treated for 48 h.[89]

Annexin V Apoptosis Assay

Annexin V-FITC/PI double staining was assayed to assess the effects elicited by TA-NE formula treatment of MDA-MB-231 cells with the determined IC_{50} of TA-NE formula in necrotic phase (Q1), late apoptotic phase (Q2), viable phase (Q3) and early apoptotic phase (Q4) as compared to that of untreated cells (Figure 9). Treatment of MDA-MB-231 cells resulted in a significant increase ($p<0.01$) in cell population in Q1 and Q2, which indicates that TA-NE formula treatment induced an increase in the necrotic as well as the late apoptotic phases.

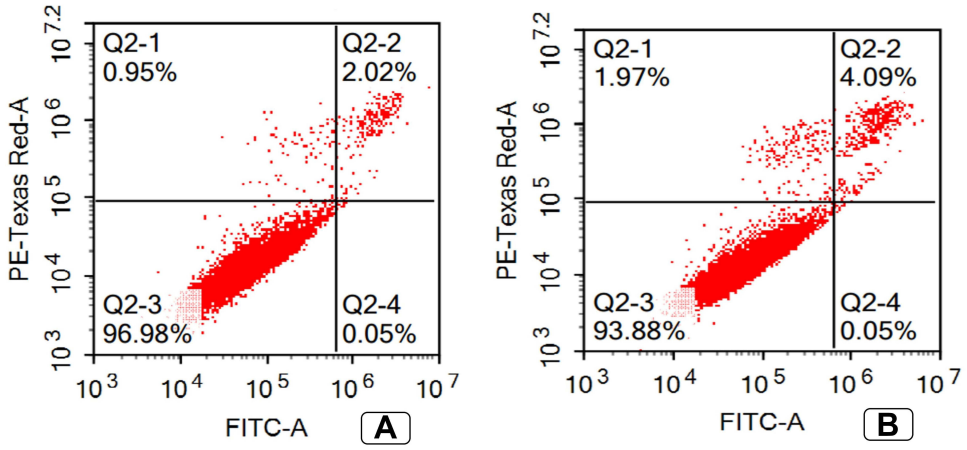

Figure 9 Annexin V apoptosis assay (**A**) Untreated MDA-MB-231 cell line; (**B**) Treated MDA-MB-231 cell line with TA-NE formula. Treated MDA-MB-231 cell line showed a significant increase in cell percentage in Q1 and Q2 representing necrotic and late apoptotic phases.

Quantification of Marker Genes' Transcripts Levels (Quantitative RT-PCR)

The present study was designed to study the antiproliferative and antiangiogenic activities of the TA-NE formula against the MDA-MB-231 cancer cell line. The effect of the TA-NE formula on the expression levels of TGF-β, MCL-1, VEGF, TNF-α, STAT3 and IL-6 mRNA in the MDA-MB-231 cell line was investigated. Figure 10 shows that the TA-NE formula resulted in a reduction in the transcript levels of TGF-β, MCL-1, VEGF, TNF-α, STAT3 and IL-6 by 2.22, 2.33, 4, 3.4, 2.4 and 4.5 folds, respectively, as compared to the transcript levels of these genes in the untreated MDA-MB-231 cell line.

VEGF is a key regulator in the prognosis of cancer. It is primarily produced by tumor cells for tumor angiogenesis. Its production is one of the most specific regulators of the angiogenic signaling cascade.[90] Moreover, the production of VEGF can be enhanced through different factors, including TNF-α and IL-6.[91] Our data reveal that the TA-NE formula resulted in a significant reduction in the transcript levels of VEGF, IL-6 and TNF-α. These results are consistent with Gupta et al,[92] who stated that THD suppressed the production of VEGF in multiple myeloma cell lines.[92] El-Aarag et al[12]

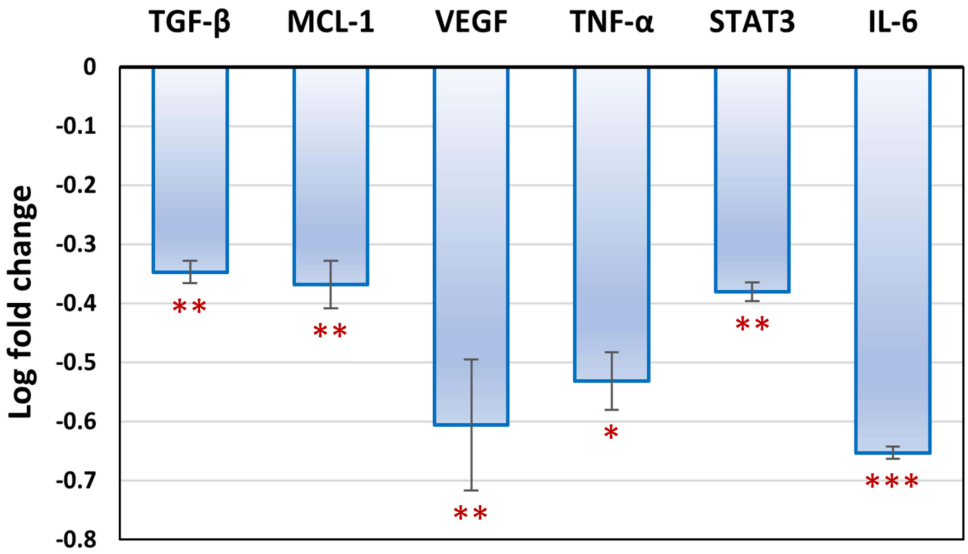

Figure 10 Gene expression analysis of TGF-β, MCL-1, VEGF, TNF-α, STAT3 and IL-6 in untreated (control) MDA-MB-231 cell line and TA-NE formula treated MDA-MB -231 cell line. TA-NE formula downregulated the expression levels of TGF-β, MCL-1, VEGF, TNF-α, STAT3 and IL-6 by 2.22, 2.33, 4, 3.4, 2.4 and 4.5 folds, respectively. Data are presented as mean ± standard deviation. Significantly (*$p < 0.05$, **$p < 0.01$, ***$p < 0.0001$).

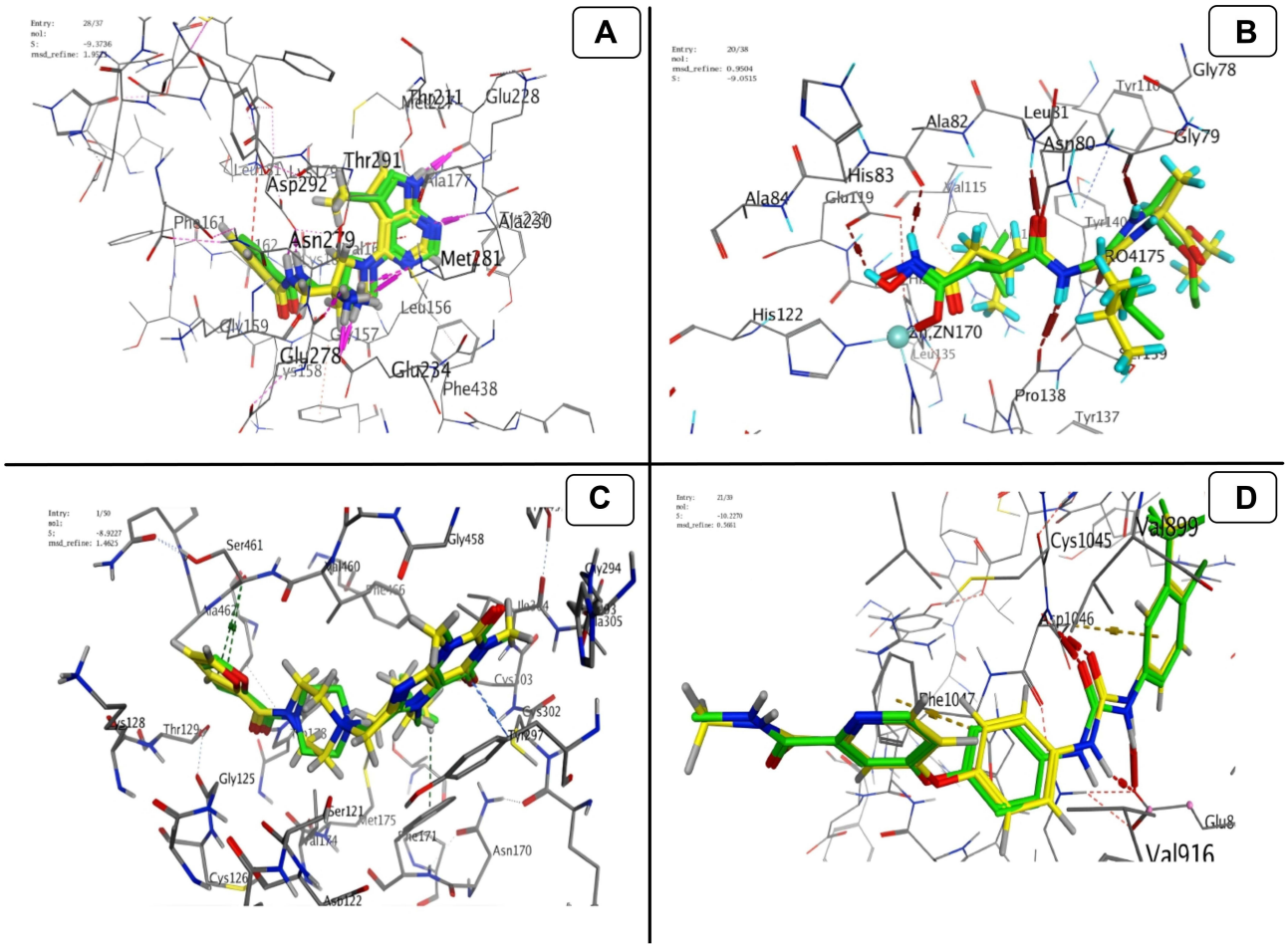

Figure 11 Validation process for docking (WFE, RO4, 3SR and BAX) into (**A**) AKT Kinase; (**B**) MMP1; (**C**) ALDH1; (**D**) VEGF, respectively. Co-crystallized ligand with green colour and the docked molecule with yellow colour.

studied the expression levels of VEGF, IL-6 and TNF-α in treated MDA-MB-231 cell line with THD and TA, and found that at a concentration of 100 μM for both THD and TA resulted in a reduction in the transcript levels of the studied mRNA but TA showed higher potency than THD.[12] THD diminished TNF-α production by enhancing TNF-α mRNA degradation.[93,94] Deng et al[95] concluded that THD inhibited TNF-α production and antigen-presenting ability of epidermal Langerhans cells at a concentration of 200 μg/mL.[95] Furthermore, the mRNA levels of VEGF were also decreased when the primary adenocarcinoma colon (SW480) cell line was treated with 50 μg/mL of THD and it showed a dose-dependent inhibitory response.[16] The mechanism by which THD exerts its role is that it blocks the NF-kB signaling pathway and the expression of inflammatory mediators, including TNF-α. Thus, NF-kB inhibits IL-6, which in turn decreases the VEGF mRNA levels and consequently leads to a reduction in angiogenesis.[96]

STAT3 is the Janus Kinase (JAK) substrate of the JAK-STAT3 pathway. It plays an important role in the signal transduction of cytokines, cellular apoptosis, proliferation, differentiation and angiogenesis.[97] GP130 is a cytokine receptor used by the IL-6 cytokine family. It forms a dimer with IL-6 and activates JAK, which leads to the activation of STAT3. The activated STAT3 forms a dimer and is translocated to the nucleus to modify the expression of target genes that affect proliferation, migration and other cellular processes, including induction of VEGF expression. Therefore, the downregulation of STAT3 would result in a reduction in VEGF expression.[98] In our study, TA-NE formula caused a reduction in IL-6 transcript level by 4.5 folds, leading to a downregulation of STAT-3 transcript level by 2.4 folds and a concomitant reduction in VEGF transcript level by 4 folds. Qian et al[99] showed that THD downregulates the expression of VEGF through STAT3/SP4 signaling pathway in a dose-dependent manner.[99]

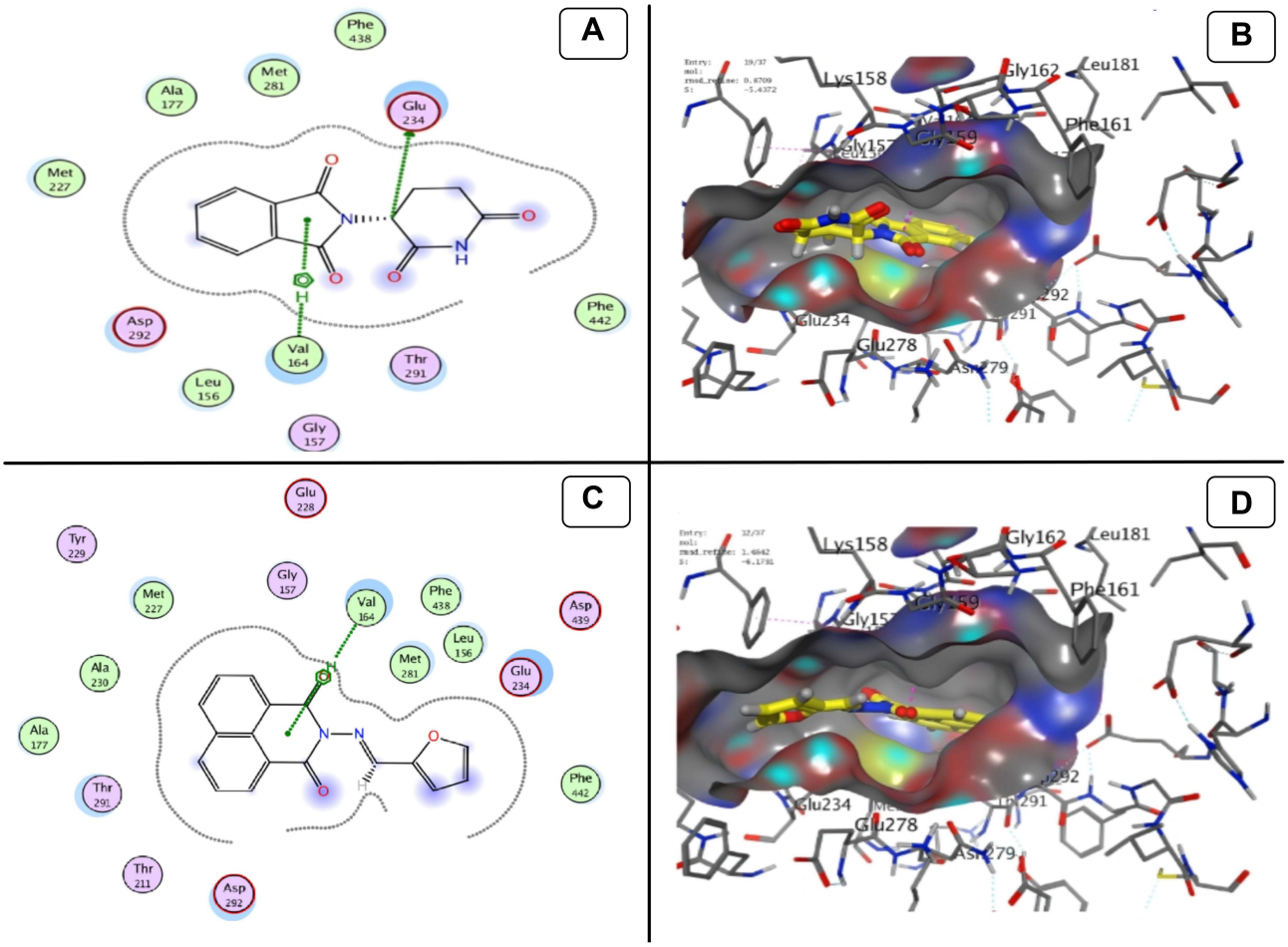

Figure 12 Docking model (**A**) 2D of THD fits into the ATP-binding site of Akt Kinase; (**B**) 3D of THD fits into the ATP-binding site of Akt Kinase; (**C**) 2D of TA fits into the ATP-binding site of Akt Kinase; (**D**) 3D of TA fits into the ATP-binding site of Akt Kinase.

In addition, Zhuang et al[100] reported that STAT3 activation in melanoma cells by Src enhanced the upregulation of MCL-1,[100] which is a member of the BCL-2 family that regulates the intrinsic apoptotic cascade. MCL-1 interacts with pro-apoptotic BCL-2 family members and causes inhibition of apoptotic mechanisms in normal and malignant cells.[101] Moreover, MCL-1 is located in the outer mitochondrial membrane; however, it can be localized to the inner mitochondrial membrane to regulate oxidative phosphorylation and maintain mitochondrial structure.[102] Zhuang group's data[100] support our results that indicate a downregulation of MCL-1 expression as a consequence of STAT3 downregulation. TA-NE downregulated STAT-3 and MCL-1 by 2.4 and 2.33 folds, respectively. Furthermore, TGF-β, a highly pleiotropic cytokine that plays an important role in angiogenesis, immunoregulation and cancer, was also downregulated by 2.22 folds. Choe et al[103] recorded that THD inhibited TGF-β mRNA levels in a dose-dependent manner in human and mouse lung fibroblast.[103] The above data indicate that TA-NE formula acts to suppress angiogenesis via downregulation of the expression of different genes that promote angiogenesis by different mechanisms.

In Silico Molecular Docking Studies

Molecular docking studies were conducted using Molecular Operating Environment software (MOE, 2014.0901). They explained the possible binding modes and molecular interactions behind the inhibitory activities of THD and TA. The top-scored conformations and favorable binding interactions were used to choose the docking poses. The docking scores, hydrogen bonds and relative placement of the docked compounds with respect to the co-crystallized ligands were used to determine the binding affinities to the investigated enzymes.

Based on the kinase activity assay results, molecular docking was performed. The IC_{50} values for AKT kinase, MMP-1, ALDH1 and VEGF were 6.627, 5.513, 5.606 and 5.393 μM, respectively. The molecular docking protocol was validated by re-docking the co-crystallized ligands; WFE (for AKT), RO4 (for MMP1), 3SR (for ALDH1) and BAX (for VEGF) into the respective enzyme binding sites. The original poses generated from PDB were regained with root mean square deviation (RMSD) values of 1.952, 1.7, 0.9504 and 0.566 Å, and binding energy scores (S score) of -9.373, -8.7242, -9.0505 and -10.227 kcal/mol, respectively (Figure 11). This demonstrates the robustness and dependability of the docking procedures utilized.

To predict the possible binding modes of THD and TA in the ATP-binding site of Akt kinase (PDB code: 3mvh), we performed molecular docking studies. Both occupied the binding pocket of the co-crystallized ligand with RMSD values of 0.8709 and 1.48 Å and binding energy scores of -5.437 and -6.17 kcal/mol, respectively (Figure 12). THD forms hydrogen bond with Glu234 and makes hydrophobic interactions with the surrounding residues, including Leu156, Ala177, Met227, Met281, Phe438 and Phe442, specially Val164, while TA makes hydrophobic interaction with Val164 and was surrounded with Leu156, Ala177, Met227, Ala230, Met281, Phe438 and Phe442.

For the molecular docking studies on MMP-1, an enzyme with PDB code: 2TCL (resolution: 2.20 Å) was selected from the protein data bank. MMP-1 belongs to the class of zinc-based metalloproteinase. The catalytic site within the enzyme has 3 histidine residues (His118, His122 and His128) in a sequence HE–H–G–H and catalytic zinc. The zinc chelating MMP-1 inhibitor (RO314724) binds within the active site which is very close to the catalytic site. The active site consists of Gly79, Leu81, Ala82, Glu119, Tyr140 and Pro138.

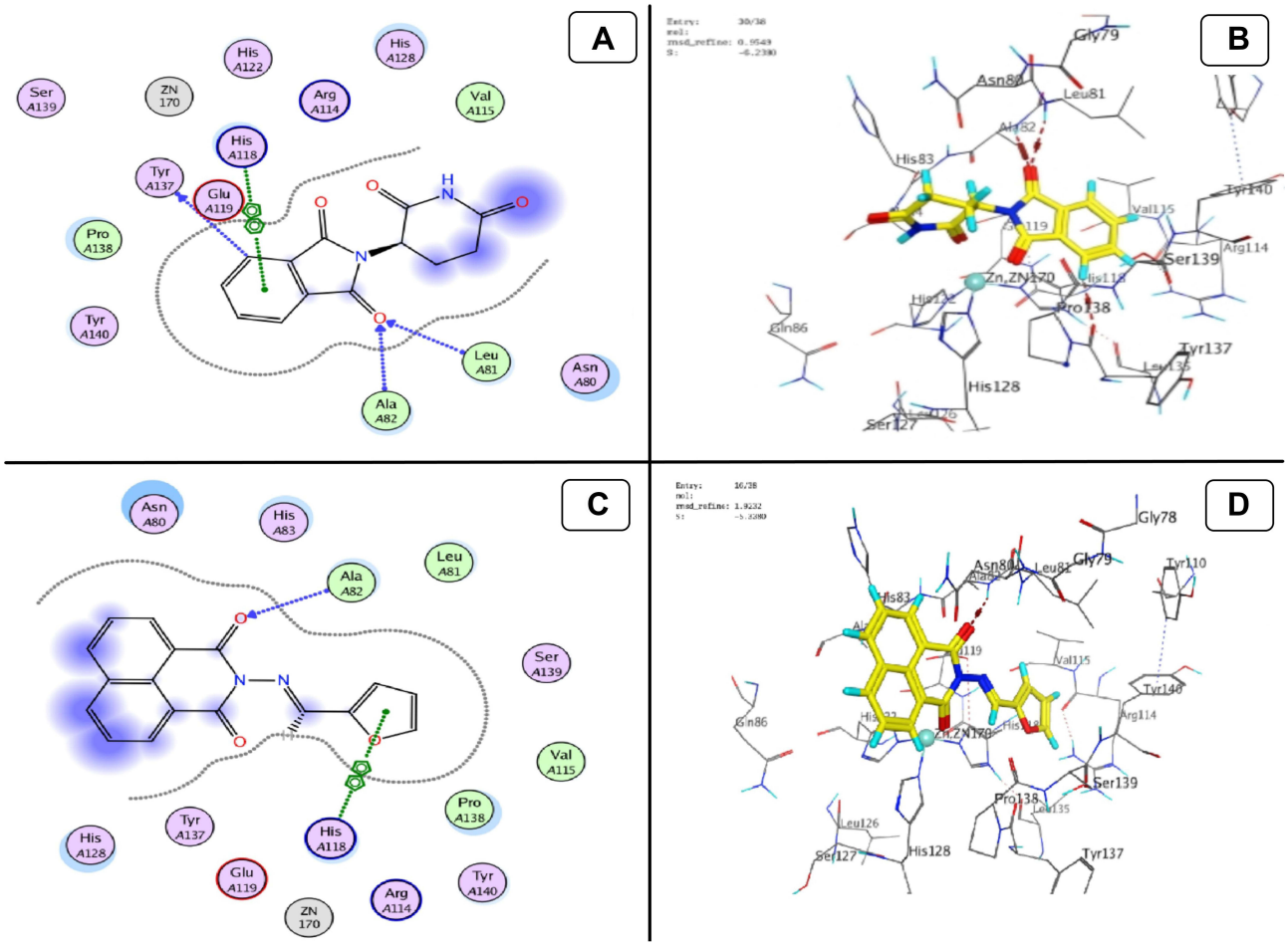

Figure 13 Docking model (**A**) 2D of THD fits into binding site of MMP-1; (**B**) 3D of THD fits into binding site of MMP-1; (**C**) 2D of TA fits into binding site of MMP-1; (**D**) 3D of TA fits into binding site of MMP-1.

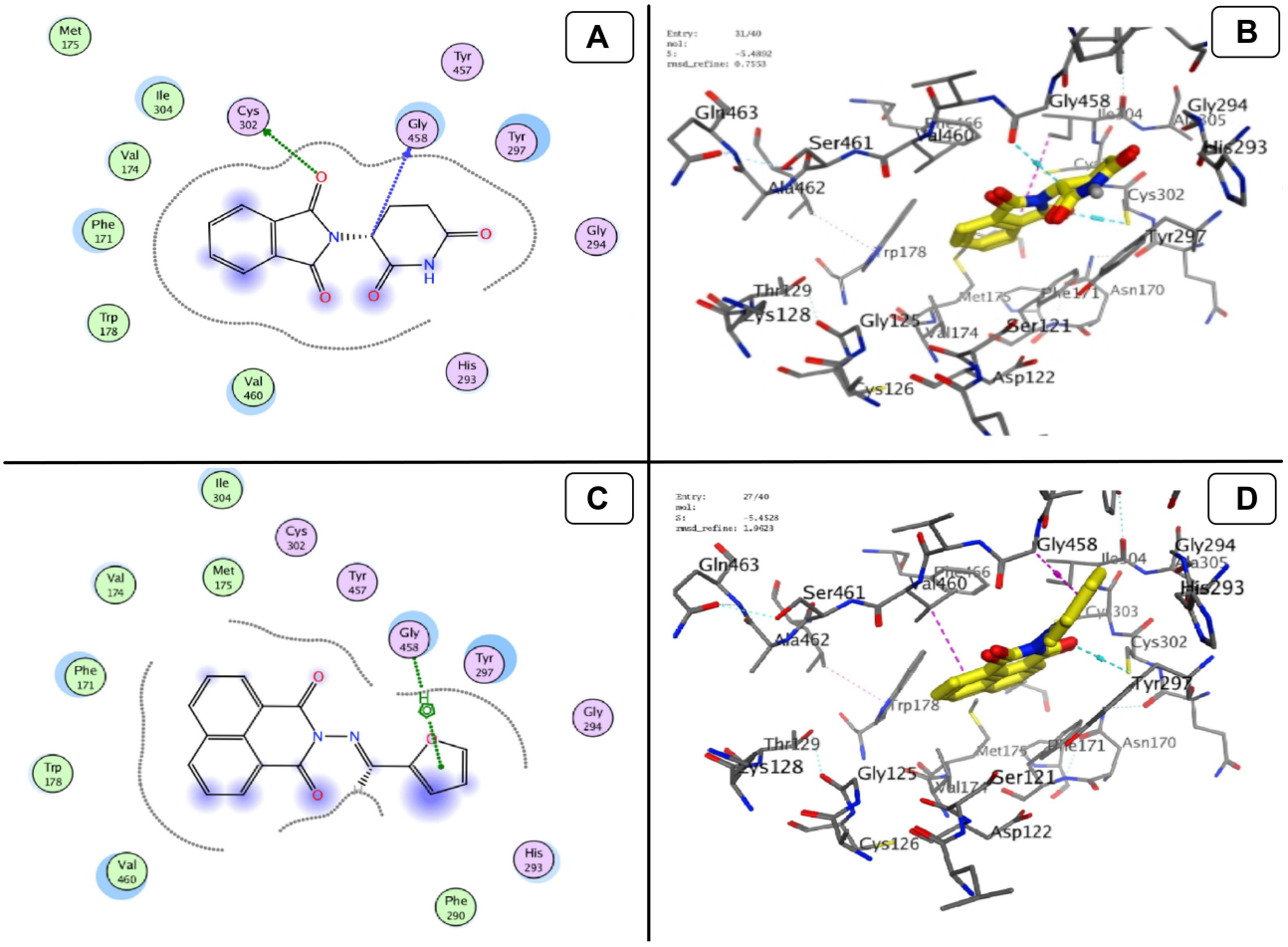

Figure 14 Docking model (**A**) 2D of THD fits into binding site of ALDH1; (**B**) 3D of THD fits into binding site of ALDH1; (**C**) 2D of TA fits into binding site of ALDH1; (**D**) 3D of TA fits into binding site of ALDH1.

THD and TA form a direct interaction in the active site and bind with docking scores of -6.2380 and -5.3380 kcal/mol and RMSD values of 0.954 and 1.9232 Å, respectively, compared to the redocked crystallized ligand RO4 with docking score of -9.0505 kcal/mol and RMSD value of 0.9504 Å. Figure 13 reveals that the examined compounds bind in the same binding pocket and perform the main amino acid interactions. Related to THD, the carbonyl of isoindole acts as H-bond acceptor and forms H-bonds with Ala82 and Leu81, and phenyl produces H-bond with Try137, and hydrophobic interaction with His118. On the other hand, the phenyl of TA produces H-bond with Ala82, but furan produces hydrophobic interaction with His118.

For the molecular docking studies on ALDH1, an enzyme with PDB code: 4WP7 was selected from the protein data bank. THD and TA form a direct interaction in the active site and bind with docking scores of -5.12 and -5.45 kcal/mol and RMSD values of 1.683 and 1.96 Å, respectively, compared to the redocked crystallized ligand 3SR with docking score of -8.7242 kcal/mol and RMSD value of 1.7 Å. Figure 14 shows that the inspected compounds bind as the same binding pocket containing polar residues (His293, Gly294, Tyr297, Cys302, Tyr457 and Gly458) and hydrophobic residues (phe171, Val174, Met175, Trp178, phe290, Ile304 and Val460) and perform the main amino acid interactions. THD forms H-bonds with Cys302 and Gly458, while TA reacts with Gly458.

Based on the obtained scoring results, THD and TA showed good binding affinity to the VEGFR-2 active site. They bind with docking scores of -5.123 and -6.023 kcal/mol and RMSD values of 1.22 and 1.75 Å, respectively, compared to the reference ligand Sorafenib with docking score of -10.227 kcal/mol and RMSD value of 0.566 Å, and form a direct interaction in the active site, like that of Sorafenib. Figure 15 reveals that the tested compounds

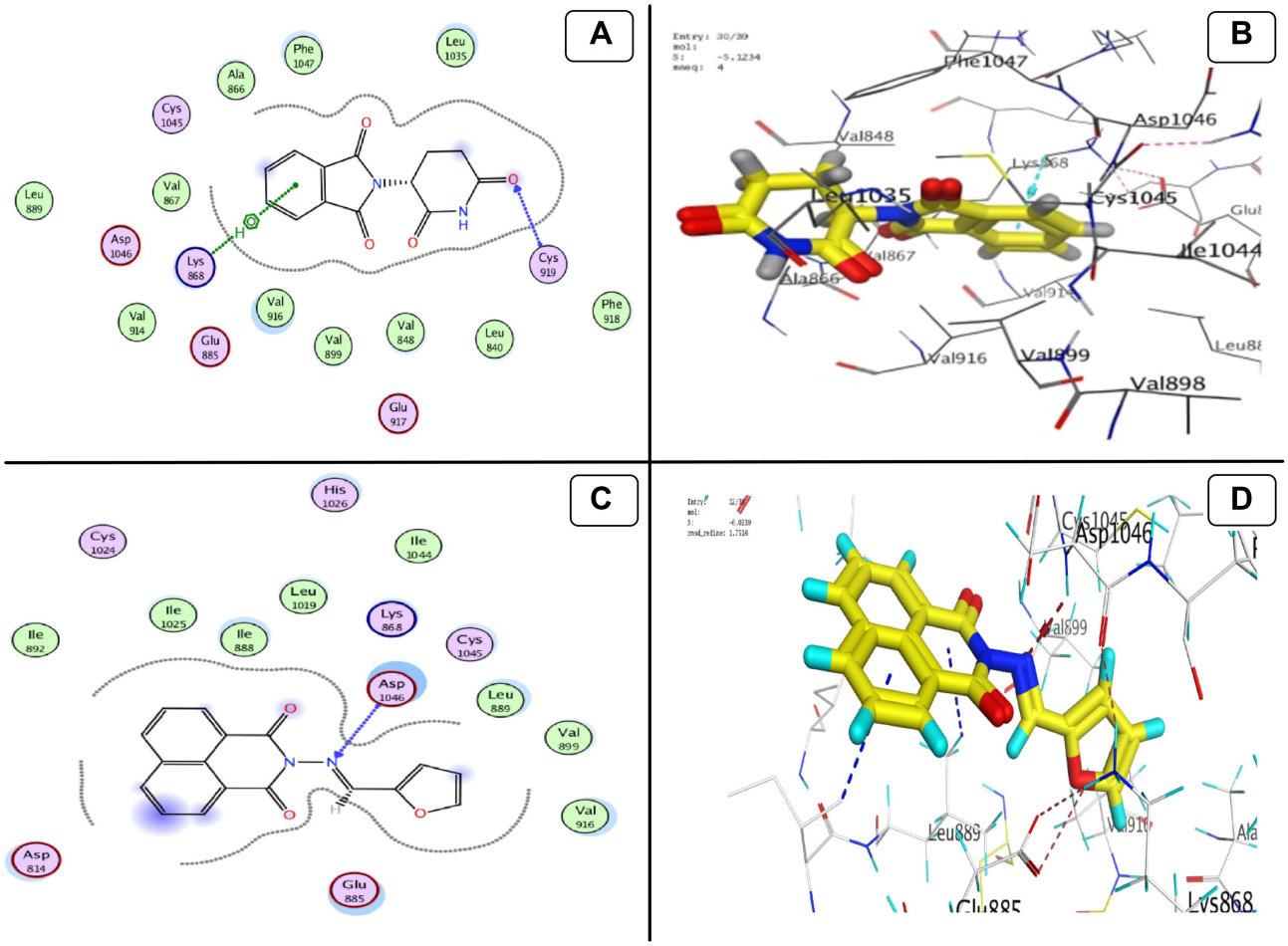

Figure 15 Docking model (**A**) 2D of THD fits into binding site of VEGF; (**B**) 3D of THD fits into binding site of VEGF; (**C**) 2D of TA fits into binding site of VEGF; (**D**) 3D of TA fits into binding site of VEGF.

bind as the same binding pocket and react with important amino acids in the active site. The carbonyl of THD acts as H-bond acceptor and forms H-bond with Cys919 and hydrophobic interaction with Lys868, while the TA imine nitrogen acts as H-bond acceptor and forms H-bond with ASP1046.

Conclusion

A novel TA was synthesized and showed cytotoxicity against different cancer cell lines. A novel nano-drug delivery system was successfully prepared that encapsulates TA and enhances its cytotoxicity. It was the first study to prepare O/W-NE using oleic acid, Tween-80, n-propyl alcohol and distilled water. The prepared TA-NE formula showed a spherical shape with a high degree of stability. FTIR spectra showed the successful encapsulation of the TA inside the formula. It is worth mentioning that the novel NE formula reduced the anticancer dosage from micromolar to nanomolar efficiency. It exhibited a concentration-dependent cytotoxicity against triple-negative breast cancer cell line. It was found that such a formula was significant in overcoming the low aqueous solubility of the TA and increased its potency. Therefore, this study is considered a significant step in formulating an effective agent for treating triple-negative breast cancer and drug-resistant breast cancer cell lines. Hence, we can conclude that the novel NE formula provides a successful loading of TA and dramatically decreases the IC_{50} of the drug to the nanomolar concentration. In addition, the prepared TA-NE formula exhibits high potency and shows a promising anticancer therapeutic efficacy for the treatment of highly metastatic and aggressive breast cancers.

Acknowledgments

This work was supported by the Ministry of Higher Education and Scientific Research (MOHE). We would like to thank Dr. Hussein Agwa (R&D Department, Pharco B Chemicals), Dr. Yara Mansour (Pharmaceutical Organic Chemistry Department, Faculty of Pharmacy, Helwan University) and Dr. Marwa Mohamed (City of Scientific Research and Technological Applications SRTA-City) for their constructive discussions.

Disclosure

Mrs Noran M Tawfik reports PhD scholarship from Ministry of Higher Education & Scientific Research, during the conduct of the study. The authors declare no other conflicts of interest in this work.

References

1. Harbeck N, Penault-Llorca F, Cortes J, et al. Breast cancer. *Nat Rev Dis Primers*. 2019;5(1):66. doi:10.1038/s41572-019-0111-2
2. Zeng K, He B, Yang BB, et al. The pro-metastasis effect of circANKS1B in breast cancer. *Mol Cancer*. 2018;17(1):1–9. doi:10.1186/s12943-018-0914-x
3. Waks AG, Winer EP. Breast cancer treatment: a review. *JAMA*. 2019;321(3):288–300. doi:10.1001/jama.2018.19323
4. Pawar A, Prabhu P. Nanosoldiers: a promising strategy to combat triple negative breast cancer. *Biomed Pharmacother*. 2019;110:319–341. doi:10.1016/j.biopha.2018.11.122
5. Chen J, Sun X, Shao R, Xu Y, Gao J, Liang W. VEGF siRNA delivered by polycation liposome-encapsulated calcium phosphate nanoparticles for tumor angiogenesis polycation liposome-encapsulated calcium phosphate nanoparticles for tumor angiogenesis inhibition in breast cancer. *Int J Nanomedicine*. 2017;12:6075–6088. doi:10.2147/IJN.S142739
6. Gao S, Wang S, Fan R, Hu J. Recent advances in the molecular mechanism of thalidomide teratogenicity. *Biomed Pharmacother*. 2020;127:110114. doi:10.1016/j.biopha.2020.110114
7. Vargesson N. Thalidomide-induced teratogenesis: history and mechanisms. *Birth Defects Res C Embryo Today*. 2015;105(2):140–156. doi:10.1002/bdrc.21096
8. Zhou S, Wang F, Hsieh TC, Wu JM, Wu E. Thalidomide – a notorious sedative to a wonder anticancer drug. *Curr Med Chem*. 2013;20(33):4102–4108. doi:10.2174/09298673113209990198
9. Huang YT, Cheng CC, Chiu TH, Lai PC. Therapeutic potential of thalidomide for gemcitabine-resistant bladder cancer. *Int J Oncol*. 2015;47(5):1711–1724. doi:10.3892/ijo.2015.3155
10. Liu Y, He S, Ding Y, Huang J, Zhang Y, Chen L. The efficacy and safety of thalidomide-based therapy in patients with advanced non-small cell lung cancer: a meta-analysis. *Contemp Oncol*. 2014;18(1):39–47. doi:10.5114/wo.2014.40782
11. Pinter M, Wichlas M, Schmid K, et al. Thalidomide in advanced hepatocellular carcinoma as antiangiogenic treatment approach: a phase I/II trial. *Eur J Gastroenterol Hepatol*. 2008;20(10):1012–1019. doi:10.1097/MEG.0b013e3283036740
12. El-Aarag BY, Kasai T, Zahran MA, et al. *In vitro* anti-proliferative and anti-angiogenic activities of thalidomide dithiocarbamate analogs. *Int Immunopharmacol*. 2014;21(2):283–292. doi:10.1016/j.intimp.2014.05.007
13. Singhal S, Mehta J. Thalidomide in cancer. *Biomed Pharmacother*. 2002;56(1):4–12. doi:10.1016/s0753-3322(01)00146-9
14. Qiao Z, Yuan J, Shen J, et al. Effect of thalidomide in combination with gemcitabine on human pancreatic carcinoma SW-1990 cell lines *in vitro* and *in vivo*. *Oncol Lett*. 2015;9(5):2353–2360. doi:10.3892/ol.2015.3064
15. Gao M, Kong Y, Wang H, et al. Thalidomide treatment for patients with previously untreated multiple myeloma: a meta-analysis of randomized controlled trials. *Tumour Biol*. 2016;37(8):11081–11098. doi:10.1007/s13277-016-4963-8
16. Zhang X, Luo H. Effects of thalidomide on growth and VEGF-A expression in SW480 colon cancer cells. *Oncol Lett*. 2018;15(3):3313–3320. doi:10.3892/ol.2017.7645
17. Ozanic Bulic S, Fassihi H, Mellerio JE, McGrath JA, Atherton DJ. Thalidomide in the management of epidermolysis bullosa pruriginosa. *Br J Dermatol*. 2005;152(6):1332–1334. doi:10.1111/j.1365-2133.2005.06492.x
18. Li C, Wang J, Wang Y, et al. Recent progress in drug delivery. *Acta Pharm Sin B*. 2019;9(6):1145–1162. doi:10.1016/j.apsb.2019.08.003
19. Balamurugan K, Chintamani P. Lipid nano particulate drug delivery: an overview of the emerging trend. *Pharma Innov J*. 2018;7(7):779–789.
20. Hu D, Ogawa K, Kajiyama M, Enomae T. Characterization of self-assembled silver nanoparticle ink based on nanoemulsion method. *R Soc Open Sci*. 2020;7(5):200296. doi:10.1098/rsos.200296
21. Xu H, Hou Z, Zhang H, et al. An efficient Trojan delivery of tetrandrine by poly (N-vinylpyrrolidone)-block-poly (ε-caprolactone) (PVP-b-PCL) nanoparticles shows enhanced apoptotic induction of lung cancer cells and inhibition of its migration and invasion. *Int J Nanomedicine*. 2014;9(1):231–242. doi:10.2147/IJN.S55541
22. Sutradhar KB, Amin ML. Nanoemulsions: increasing possibilities in drug delivery. *Eur J Nanomed*. 2013;5(2):97–110. doi:10.1515/ejnm-2013-0001
23. Chime SA, Kenechukwu FC, Attama AA. Nanoemulsions — advances in formulation, characterization and applications in drug delivery. *Appl Nanotechnol Drug Deliv*. 2014;3:77–126. doi:10.5772/15371
24. Izadiyan Z, Basri M, Fard Masoumi HR, Abedi Karjiban R, Salim N, Shameli K. Modeling and optimization of nanoemulsion containing Sorafenib for cancer treatment by response surface methodology. *Chem Cent J*. 2017;1(1):1–9. doi:10.1186/s13065-017-0248-6
25. Handa M, Ujjwal RR, Vasdev N, Flora S, Shukla R. Optimization of surfactant- and cosurfactant-aided pine oil nanoemulsions by isothermal low-energy methods for anticholinesterase activity. *ACS omega*. 2020;6(1):559–568. doi:10.1021/acsomega.0c05033

26. Sobhani H, Tarighi P, Ostad SN, Shafaati A, Nafissi-Varcheh N, Aboofazeli R. Formulation development and toxicity assessment of triacetin mediated nanoemulsions as novel delivery systems for rapamycin. *Iran J Pharm Res*. 2015;14(Suppl):3. doi:10.22037/IJPR.2015.1708
27. Boonme P, Krauel K, Graf A, Rades T, Junyaprasert VB. Characterization of microemulsion structures in the pseudoternary phase diagram of isopropyl palmitate/water/Brij 97:1-butanol. *AAPS PharmSciTech*. 2006;7(2):E99–104. doi:10.1208/pt070245
28. Kawakami K, Yoshikawa T, Hayashi T, Nishihara Y, Masuda K. Microemulsion formulation for enhanced absorption of poorly soluble drugs. II. *In* vivo study. *J Control Release*. 2002;81(1–2):75–82. doi:10.1016/s0168-3659(02)00050-0
29. McClements DJ, Rao J. Food-grade nanoemulsions: formulation, fabrication, properties, performance, biological fate, and potential toxicity. *Crit Rev Food Sci Nutr*. 2011;51(4):285–330. doi:10.1080/10408398.2011.559558
30. Sánchez-López E, Guerra M, Dias-Ferreira J, et al. Current applications of nanoemulsions in cancer therapeutics. *Nanomaterials*. 2019;9 (6):821. doi:10.3390/nano9060821
31. Moura JA, Valduga CJ, Tavares ER, Kretzer IF, Maria DA, Maranhão RC. Novel formulation of a methotrexate derivative with a lipid nanoemulsion. *Int J Nanomedicine*. 2011;6:2285–2295.
32. Singh Y, Meher JG, Raval K, et al. Nanoemulsion: concepts, development and applications in drug delivery. *J Control Release*. 2017;252:28–49. doi:10.1016/j.jconrel.2017.03.008
33. Natesan S, Sugumaran A, Ponnusamy C, Thiagarajan V, Palanichamy R, Kandasamy R. Chitosan stabilized camptothecin nanoemulsions: development, evaluation and biodistribution in preclinical breast cancer animal mode. *Int J Biol Macromol*. 2017;104:1846.
34. Periasamy VS, Athinarayanan J, Alshatwi AA. Anticancer activity of an ultrasonic nanoemulsion formulation of Nigella sativa L. essential oil on human breast cancer cells. *Ultrason Sonochem*. 2016;31:449–455. doi:10.1016/j.ultsonch.2016.01.035
35. Chaudhari PM, Kuchekar MA. Development and evaluation of nanoemulsion as a carrier for topical delivery system by box-behnken design. *Asian J Pharm Clin Res*. 2018;11:286–293. doi:10.22159/ajpcr.2018.v11i8.26359
36. Aswathanarayan JB, Vittal RR. Nanoemulsions and their potential applications in food industry. *Front Sustain Food Syst*. 2019;3:95. doi:10.3389/fsufs.2019.00095
37. Tsai J, Fu S, Lin H, Huang B, Wu C. The effect of nanoemulsion as a carrier of hydrophilic compound for transdermal delivery. *PLoS One*. 2014;9(7):e102850. doi:10.1371/journal.pone.0102850
38. Azeem A, Rizwan M, Ahmad FJ, et al. Nanoemulsion components screening and selection: a technical note. *AAPS PharmSciTech*. 2009;10 (1):69–76. doi:10.1208/s12249-008-9178-x
39. Sarheed O, Dibi M, Ramesh K. Studies on the effect of oil and surfactant on the formation of alginate-based O/W lidocaine nanocarriers using nanoemulsion template. *Pharmaceutics*. 2020;12(12):1223. doi:10.3390/pharmaceutics12121223
40. Anton N, Benoit JP, Saulnier P. Design and production of nanoparticles formulated from nano-emulsion templates—a review. *J Control Release*. 2008;128(3):185–199. doi:10.1016/j.jconrel.2008.02.007
41. Khashan KS, Abdulameer FA, Jabir MS, Hadi AA, Sulaiman GM. Anticancer activity and toxicity of carbon nanoparticles produced by pulsed laser ablation of graphite in water. *Adv Nat Sci*. 2020;11(3):035010. doi:10.1088/2043-6254/aba1de
42. Choi SJ, McClements DJ. Nanoemulsions as delivery systems for lipophilic nutraceuticals: strategies for improving their formulation, stability, functionality and bioavailability. *Food Sci Biotechnol*. 2020;29(2):149–168. doi:10.1007/s10068-019-00731-4
43. Wu HR, Wang CQ, Wang JX, Chen JF, Le Y. Engineering of long-term stable transparent nanoemulsion using high-gravity rotating packed bed for oral drug delivery. *Int J Nanomedicine*. 2020;15:2391–2402. doi:10.2147/IJN.S238788
44. Alliod O, Valour J, Urbaniak S, Fessi H, Dupin D, Charcosset C. Preparation of oil-in-water nanoemulsions at large-scale using premix membrane emulsification and Shirasu Porous Glass (SPG) membranes. *Colloids Surf a Physicochem*. 2018;557:76–84. doi:10.1016/j.colsurfa.2018.04.045
45. Dash S, Murthy PN, Nath L, Chowdhury P. Kinetic modeling on drug release from controlled drug delivery systems. *Acta Pol Pharm*. 2010;67 (3):217–223.
46. Al-Salman H, Ali ET, Jabir M, Sulaiman GM, Al-Jadaan SA. 2-Benzhydrylsulfinyl-N-hydroxyacetamide-Na extracted from fig as a novel cytotoxic and apoptosis inducer in SKOV-3 and AMJ-13 cell lines via P53 and caspase-8 pathway. *Eur Food Res Technol*. 2020;246 (8):1591–1608. doi:10.1007/s00217-020-03515-x
47. Al-Ziaydi AG, Al-Shammari AM, Hamzah MI, Kadhim HS, Jabir MS. Newcastle disease virus suppress glycolysis pathway and induce breast cancer cells death. *Virusdisease*. 2020;31(3):341–348. doi:10.1007/s13337-020-00612-z
48. Meerloo JV, Kaspers GJ, Cloos J. Cell sensitivity assays: the MTT assay. *Methods Mol Biol*. 2011;731:237–245. doi:10.1007/978-1-61779-080-5_20
49. Ibrahim AA, Kareem MM, Al-Noor TH, et al. Pt (II)-thiocarbohydrazone complex as cytotoxic agent and apoptosis inducer in Caov-3 and HT-29 Cells through the P53 and caspase-8 pathways. *Pharmaceuticals*. 2021;14(6):509. doi:10.3390/ph14060509
50. Al-Shammari AM, Al-Saadi H, Al-Shammari SM, Jabir MS. Galangin enhances gold nanoparticles as anti-tumor agents against ovarian cancer cells. *AIP Conf Proc*. 2020;2213(1):020206.
51. DTP. Developmental Therapeutics Program; 2022. Available from: https://dtp.cancer.gov/organization/dscb/compoundSubmission/structureSelection.htm. Accessed December 28, 2022.
52. Tawfik NM, Teiama M, Iskandar SS, Osman A, Hammad SF. Formulation and characterization of a thalidomide analogue in nanoemulsion system. *Int J Pharma Med Biol Sci*. 2022;11(2):43–47. doi:10.18178/ijpmbs.11.2.43-47
53. Prabhakar K, Afzal SM, Surender G, Kishan V. Tween 80 containing lipid nanoemulsions for delivery of indinavir to brain. *Acta Pharm Sin B*. 2013;3(5):345–353. doi:10.1016/j.apsb.2013.08.001
54. Jiang L, Wang W, He Q, et al. Oleic acid induces apoptosis and autophagy in the treatment of Tongue Squamous cell carcinomas. *Sci Rep*. 2017;7(1):1–11. doi:10.1038/s41598-017-11842-5
55. Manickam S, Sivakumar K, Pang CH. Investigations on the generation of oil-in-water (O/W) nanoemulsions through the combination of ultrasound and microchannel. *Ultrason Sonochem*. 2020;69:105258. doi:10.1016/j.ultsonch.2020.105258
56. Jaiswal M, Dudhe R, Sharma PK. Nanoemulsion: an advanced mode of drug delivery system. *Biotech*. 2015;5(2):123–127. doi:10.1007/s13205-014-0214-0
57. Rao J, McClements DJ. Lemon oil solubilization in mixed surfactant solutions: rationalizing microemulsion & nanoemulsion formation. *Food Hydrocoll*. 2012;26(1):268–276. doi:10.1016/j.foodhyd.2011.06.002

58. Dalvi SV, Dave RN. Controlling particle size of a poorly water-soluble drug using ultrasound and stabilizers in antisolvent precipitation. *Ind Eng Chem Res*. 2009;48(16):7581. doi:10.1021/ie900248f
59. Shah AV, Desai HH, Thool P, Dalrymple D, Serajuddin AT. Development of self-microemulsifying drug delivery system for oral delivery of poorly water-soluble nutraceuticals. *Drug Dev Ind Pharm*. 2018;44(6):895–901. doi:10.1080/03639045.2017.1419365
60. Mathew DS, Juang RS. Role of alcohols in the formation of inverse microemulsions and back extraction of proteins/enzymes in a reverse micellar system. *Sep Purif Technol*. 2007;53(3):199–215. doi:10.1016/j.seppur.2006.10.001
61. Wang L, Zhang Y. Eugenol nanoemulsion stabilized with zein and sodium caseinate by self-assembly. *J Agric Food Chem*. 2017;65 (14):2990–2998. doi:10.1021/acs.jafc.7b00194
62. Danaei M, Dehghankhold M, Ataei S, et al. Impact of particle size and polydispersity index on the clinical applications of lipidic nanocarrier systems. *Pharmaceutics*. 2018;10(2):57. doi:10.3390/pharmaceutics10020057
63. Pouton CW. Lipid formulations for oral administration of drugs: non-emulsifying, self-emulsifying and 'self-microemulsifying' drug delivery systems. *Eur J Pharm Sci*. 2000;11:S93–98. doi:10.1016/s0928-87(00
64. Wang C, Cui B, Guo L, et al. Fabrication and evaluation of lambda-cyhalothrin nanosuspension by one-step melt emulsification technique. *Nanomaterials*. 2019;9(2):145. doi:10.3390/nano9020145
65. Sanson N, Bouyer F, Destarac M, In M, Gerardin C. Hybrid polyion complex micelles formed from double hydrophilic block copolymers and multivalent metal ions: size control and nanostructure. *Langmuir*. 2012;28(8):3773–3782. doi:10.1021/la204562t
66. Sun B, Yeo Y. Nanocrystals for the parenteral delivery of poorly water-soluble drugs. *Curr Opin Solid State Mater Sci*. 2012;16(6):295–301. doi:10.1016/j.cossms.2012.10.004
67. Wei XL, Han YR, Quan LH, Liu CY, Liao YH. Oily nanosuspension for long-acting intramuscular delivery of curcumin didecanoate prodrug: preparation, characterization and *in vivo* evaluation. *Eur J of Pharm Sci*. 2013;49(2):286–293. doi:10.1016/j.ejps.2013.03.010
68. Wani TA, Masoodi FA, Jafari SM, McClements DJ. Safety of nanoemulsions and their regulatory status. *Nanoemulsions*. 2018;613–628. doi:10.1016/B978-0-12-811838-2.00019-9
69. Wang L, Du J, Zhou Y, Wang Y. Safety of nanosuspensions in drug delivery. *Nanomedicine*. 2017;13(2):455–469. doi:10.1016/j.nano.2016.08.007
70. Attia MF, Anton N, Wallyn J, Omran Z, Vandamme TF. An overview of active and passive targeting strategies to improve the nanocarriers efficiency to tumour sites. *J Pharm Pharmacol*. 2019;71(8):1185–1198.
71. Maeda H. The enhanced permeability and retention (EPR) effect in tumor vasculature: the key role of tumor-selective macromolecular drug targeting. *Adv Enzyme Regul*. 2001;41:189–207. doi:10.1016/s0065-2571(00
72. Jin H, Hemingway M, Gupta RB, Xia F, Zhao Y. Preparation of thalidomide nano-flakes by supercritical antisolvent with enhanced mass transfer. *Particuology*. 2012;10(1):17–23. doi:10.1016/j.partic.2011.05.003
73. Che Marzuki NH, Wahab RA, Abdul Hamid M. An overview of nanoemulsion: concepts of development and cosmeceutical applications. *Biotechnol Biotechnol Equip*. 2019;33(1):779–797. doi:10.1080/13102818.2019.1620124
74. Danhier F, Feron O, Préat V. To exploit the tumor microenvironment: passive and active tumor targeting of nanocarriers for anti-cancer drug delivery. *J Control Release*. 2010;148(2):135–146. doi:10.1016/j.jconrel.2010.08.027
75. Li Y, Liu B, Jiang L, et al. Interaction of soybean protein isolate and phosphatidylcholine in nanoemulsions: a fuorescence analysis. *Food Hydrocoll*. 2019;87:814–829. doi:10.1016/j.foodhyd.2018.09.006
76. Rodrigues FV, Diniz LS, Sousa RM, et al. Preparation and characterization of nanoemulsion containing a natural naphthoquinone. *Quím Nova*. 2018;41:756–761. doi:10.21577/0100-4042.20170247
77. Tran TH, Ramasamy T, Truong DH, et al. Development of vorinostat-loaded solid lipid nanoparticles to enhance pharmacokinetics and efficacy against multidrug-resistant cancer cells. *Pharm Res*. 2014;31(8):1978–1988.
78. Kang JH, Chon J, Kim YI, et al. Preparation and evaluation of tacrolimus-loaded thermosensitive solid lipid nanoparticles for improved dermal distribution. *Int J Nanomedicine*. 2019:5381–5396. doi:10.2147/IJN.S215153
79. Xu X, Khan MA, Burgess DJ. A two-stage reverse dialysis *in vitro* dissolution testing method for passive targeted liposomes. *Int J Pharm*. 2012;426(1–2):211–218. doi:10.1016/j.ijpharm.2012.01.030
80. Araújo FA, Kelmann RG, Araújo BV, Finatto RB, Teixeira HF, Koester LS. Development and characterization of parenteral nanoemulsions containing thalidomide. *Eur J Pharm Sci*. 2011;42(3):238–245. doi:10.1016/j.ejps.2010.11.014
81. Sun W, Ma X, Wei X, Xu Y. Nano composite emulsion for sustained drug release and improved bioavailability. *Pharm Res*. 2014;31 (10):2774–2783. doi:10.1007/s11095-014-1374-7
82. Chen M, Sun H, Zhao Y, et al. Comparison of patterns and prognosis among distant metastatic breast cancer patients by age groups: a SEER population-based analysis. *Sci Rep*. 2017;7(1):1–8. doi:10.1038/s41598-017-10166-8
83. Weigelt B, Peterse JL, van 't Veer LJ. Breast cancer metastasis: markers and models. *Nat Rev Cancer*. 2005;5(8):591–602. doi:10.1038/nrc1670
84. Plonczak AM, DiMarco AN, Dina R, Gujral DM, Palazzo FF. Breast cancer metastases to the thyroid gland – an uncommon sentinel for diffuse metastatic disease: a case report and review of the literature. *J Med Case Rep*. 2017;11(1):269. doi:10.1186/s13256-017-1441-x
85. Marriott JB, Clarke IA, Czajka A, et al. A novel subclass of thalidomide analogue with anti-solid tumor activity in which caspase-dependent apoptosis is associated with altered expression of bcl-2 family proteins. *Cancer Res*. 2003;63(3):593–599.
86. El-Zahabi MA, Sakr H, El-Adl K, et al. Design, synthesis, and biological evaluation of new challenging thalidomide analogs as potential anticancer immunomodulatory agents. *Bioorg Chem*. 2020;104:104218. doi:10.1016/j.bioorg.2020
87. Zhu J, Yang Y, Liu S, et al. Anticancer effect of thalidomide *in vitro* on human osteosarcoma cells. *Oncol Rep*. 2016;36(6):3545–3551.
88. Tokunaga E, Akiyama H, Soloshonok VA, Inoue Y, Hara H, Shibata N. Biological evaluation of both enantiomers of fluoro-thalidomide using human myeloma cell line H929 and others. *PLoS One*. 2017;12(8):e0182152. doi:10.1371/journal.pone.0182152
89. Kian MM, Salemi M, Bahadoran M, et al. Curcumin combined with thalidomide reduces expression of STAT3 and Bcl-xL, leading to apoptosis in acute myeloid leukemia cell lines. *Drug Des Devel Ther*. 2020;14:185–194. doi:10.2147/DDDT.S228610
90. Ferrara N. VEGF and the quest for tumour angiogenesis factors. *Nat Rev Cancer*. 2002;2(10):795–803. doi:10.1038/nrc909
91. Neufeld G, Cohen T, Gengrinovitch S, Poltorak Z. Vascular endothelial growth factor (VEGF) and its receptors. *FASEB J*. 1999;13(1):9–22. doi:10.1096/fasebj.13.1.9

92. Gupta D, Treon SP, Shima Y, et al. Adherence of multiple myeloma cells to bone marrow stromal cells upregulates vascular endothelial growth factor secretion: therapeutic applications. *Leukemia*. 2001;15(12):1950–1961.
93. Majumder S, Rama Chaitanya Sreedhara S, Banerjee S, Chatterjee S. TNF α signaling beholds thalidomide saga: a review of mechanistic role of TNF-α signaling under thalidomide. *Curr Top Med Chem*. 2012;12(13):1456–1467. doi:10.2174/156802612801784443
94. Moreira AL, Sampaio EP, Zmuidzinas A, Frindt P, Smith KA, Kaplan G. Thalidomide exerts its inhibitory action on tumor necrosis factor alpha by enhancing mRNA degradation. *J Exp Med*. 1993;177(6):1675–1680.
95. Deng L, Ding W, Granstein RD. Thalidomide inhibits tumor necrosis factor-alpha production and antigen presentation by Langerhans cells. *J Invest Dermatol*. 2003;121(5):1060–1065.
96. de Oliveira Hernandez M, de Oliveira Fulco T, Pinheiro RO, et al. Thalidomide modulates Mycobacterium leprae-induced NF-κB pathway and lower cytokine response. *Eur J Pharmacol*. 2011;670(1):272–279. doi:10.1016/j.ejphar.2011.08.046
97. Guanizo AC, Fernando CD, Garama DJ, Gough DJ. STAT3: a multifaceted oncoprotein. *Growth Fact*. 2018;36(1–2):1–14. doi:10.1080/08977194.2018.1473393
98. Zhu N, Wang L, Guo H, et al. Thalidomide suppresses angiogenesis through the signal transducer and activator of transcription 3/SP4 signaling pathway in the peritoneal membrane. *Front Physiol*. 2021;12:712147. doi:10.3389/fphys.2021
99. Qian S, Somlo G, Zhou B, Yen Y. Therapeutic effects of thalidomide in myeloma are associated with the expression of fibroblast growth factor receptor 3. *Ther Clin Risk Manag*. 2005;1(3):231–241.
100. Zhuang L, Lee CS, Scolyer RA, et al. Mcl-1, Bcl-XL and Stat3 expression are associated with progression of melanoma whereas Bcl-2, AP-2 and MITF levels decrease during progression of melanoma. *Mod Pathol*. 2007;20(4):416–426. doi:10.1038/modpathol.3800750
101. Young AI, Law AM, Castillo L, et al. MCL-1 inhibition provides a new way to suppress breast cancer metastasis and increase sensitivity to dasatinib. *Breast Cancer Res*. 2016;18(1):125. doi:10.1186/s13058-016-0781-6
102. Perciavalle RM, Stewart DP, Koss B, et al. Anti-apoptotic MCL-1 localizes to the mitochondrial matrix and couples mitochondrial fusion to respiration. *Nat Cell Biol*. 2012;14(6):575–583. doi:10.1038/ncb2488
103. Choe JY, Jung HJ, Park KY, et al. Anti-fibrotic effect of thalidomide through inhibiting TGF-beta-induced ERK1/2 pathways in bleomycin-induced lung fibrosis in mice. *Inflamm Res*. 2010;59(3):177–188. doi:10.1007/s00011-009-0084-9